Electronic Supporting Information

Reduction of CO_2 by a Masked Two-Coordinate Cobalt(I) Complex and Characterization of a Proposed Oxodicobalt(II) Intermediate

Lisa Roy,[a,g,†] Malik H. Al-Afyouni,[b,†] Daniel E. DeRosha,[c,†] Bhaskar Mondal,[a] Ida M. DiMucci,[d] Kyle M. Lancaster,[d] Jason Shearer,[e] Eckhard Bill,[a] William W. Brennessel,[b] Frank Neese,[f] Shengfa Ye,[f,] and Patrick L. Holland[c,*]*

[a.] *Max Planck Institute for Chemical Energy Conversion, Stiftstraße 34-36, Mülheim an der Ruhr, D-45470, Germany.*
[b.] *Department of Chemistry, University of Rochester, Rochester, New York 14618, USA.*
[c.] *Department of Chemistry, Yale University, New Haven, Connecticut 06520, USA.*
[d.] *Department of Chemistry and Chemical Biology, Baker Laboratory, Cornell University, Ithaca, New York 14853, USA.*
[e.] *Department of Chemistry, University of Nevada, Reno, Nevada 89557, USA.*
[f.] *Max Planck Institute for Coal Research, Kaiser-Wilhelm-Platz 1, Mülheim an der Ruhr, D-45470, Germany*
[g.] *CSIR Central Mechanical Engineering Research Institute, Durgapur 713209, India.*

† *These authors contributed equally.*

*Shengfa Ye, email: shengfa.ye@kofo.mpg.de

*Patrick L. Holland, email: patrick.holland@yale.edu

Table of Contents

A. Experimental Section

General Considerations. All synthetic manipulations were performed under an argon atmosphere using standard Schlenk techniques or in an M. Braun glovebox maintained at or below 1 ppm O_2 and H_2O. Glassware was dried at 150 °C overnight. Hexane and toluene were purified by passage through activated alumina and Q5 columns from Glass Contour Co. (Laguna Beach, CA). Celite was dried at 300 °C under vacuum overnight. THF was dried by distilling from Na/benzophenone. THF-d_8, C_6D_{12}, and C_6D_6 were dried over CaH_2 and then over Na/benzophenone and vacuum transferred and stored over 3 Å molecular sieves. CO_2, CO, and N_2O were purchased from Airgas, Inc. and passed through a column of activated alumina. ^{13}CO was purchased from Cambridge Isotope Laboratories, Inc. $L^{tBu}CoCl$,[1] $L^{tBu}Co$,[2] and $L^{tBu}Co(CO)_2$[2,3] were synthesized according to published procedures.

^1H NMR spectra were recorded on a Bruker Avance 500 MHz spectrometer. All spectra are referenced to residual protiated solvent signals: C_6D_6 (7.16 ppm), THF-d_8 (3.58 or 1.73 ppm), C_6D_{12} (1.38 ppm). The NMR probe temperature was calibrated using methanol. IR spectra were recorded on a Shimadzu FTIR spectrophotometer (FTIR-8400S). UV-vis absorption spectra were recorded on a Cary 50 or Cary 60 spectrophotometer using Teflon-sealed quartz cuvettes. Elemental analyses were obtained from the CENTC Elemental Analysis Facility at the University of Rochester. Microanalysis samples were handled under argon, weighed with a PerkinElmer Model AD-6 Autobalance, and their compositions were determined with a PerkinElmer 2400 Series II Analyzer.

Reaction of $L^{tBu}Co$ with CO_2. A resealable flask was charged with $L^{tBu}Co$ (158 mg, 0.28 mmol) and hexane (15 mL). The dark solution was frozen with liquid N_2 and the headspace of the flask was evacuated. While submerged in liquid N_2, CO_2 (7.73 mL at 891 mBar, 0.28 mmol) was introduced to the flask and allowed to condense for 30 min. The solution was allowed to thaw at room temperature before stirring at 60 °C for 11 h to give a red solution.

The solution was filtered through Celite, and volatiles were removed to give a red solid mixture of **2** and **4**. Cold pentane (5 mL) was used to extract **2**. The volume was reduced to ~2 mL, and cooling the solution to -40 °C caused crystalline **2** to precipitate (36 mg, 66%). The spectroscopic characteristics of **2** ($L^{tBu}CoCO$) matched the literature.[3] The remaining solid residue was extracted with toluene (10 mL) and the volume was reduced to ~5 mL. Cooling to -40 °C gave crystals of **4** (44 mg, 40%). Characterization of **4**: ^{1}H NMR (500 MHz, C_6D_6): δ 26.8 (36H, t-Bu), 23.0 (8H, *m*-Ar), -4.8 (12H, iPr-C*H*$_3$), -6.9 (2H, backbone-C*H*), -41.0 (4H, iPr-C*H*), -45.4 (4H, *p*-Ar), -48.8 (12H, iPr-C*H*$_3$). Anal. Calcd. for $C_{71}H_{106}N_4O_3Co_2$: C, 72.22; H, 9.05; N, 4.74. Found: C, 72.42; H, 9.09; N, 4.51.

Synthesis of $[L^{tBu}Co]_2(\mu\text{-}O)$ (3). A resealable flask was charged with $L^{tBu}Co$ (348.0 mg, 0.6206 mmol) and hexanes (50 mL). The dark brown solution was frozen using a liquid N_2 bath, and the headspace of the flask was evacuated. While frozen, N_2O (13.34 mL at 633 mbar, 0.341 mmol) was introduced to the flask and condensed for 30 min. The solution was thawed and stirred at -78 °C for 4 h and then at ambient temperature for 2 h, resulting in precipitation of a red-orange solid. The mixture was filtered through Celite to collect red-orange solid. This solid was washed with hexanes (20 mL), extracted into THF (30 mL), and dried under vacuum to afford crude **3** (228.6 mg, 65%). Analytically pure **3** was obtained by dissolving 76 mg of crude **3** in THF (10 mL), concentrating the red solution to 5 mL under vacuum, and storing at -40 °C overnight to yield crystals. Single crystals for crystallography were grown by slowly evaporating a concentrated toluene solution under reduced pressure. ^{1}H NMR (C_6D_6): δ 34.0 (br), 12.8, -20.5 (br), -34.0 ppm. μ_{eff} (C_6D_6, 25 °C) 4.4(1) μ_B. IR (KBr): 3049 (w), 2958 (s), 2922 (m), 2900 (m), 2865 (m), 1596 (w), 1539 (m), 1488 (m), 1457 (m), 1429 (m), 1383 (s), 1361 (s), 1309 (m), 1250 (m), 1202 (m), 1179 (m), 1152 (w), 1098 (m), 1018 (w) cm^{-1}. Anal. Calcd for $C_{70}H_{106}N_4OCo_2$: C, 73.92; H, 9.39; N, 4.92. Found: C, 73.54; H, 9.52; N, 4.54.

NMR-scale reaction of 3 with CO_2. A vial was charged with **3** (2.0 mg, 0.0018 mmol) and 1.0 mL C_6D_{12}. The orange mixture was stirred vigorously for 5 min before transfering 0.5 mL of this solution to a J. Young NMR tube containing a capillary with a nickelocene integration standard. The J. Young tube was sonicated for 1 min, and then the contents of the tube were flash frozen in a liquid N_2 cold bath. The headspace of the tube was evacuated. While frozen, CO_2 (13.34 mL at 5 mbar) was introduced to the tube and condensed for 30 min. The solution was thawed and then immediately injected into an NMR spectrometer cooled to 10 °C. NMR analysis using a nickelocene integration standard indicated formation of **4** in 75% spectroscopic yield (see Figure S5).

Computational details. Geometry optimizations utilized the unrestricted Kohn Sham theory and employed the GGA density functional BP86[4, 5] in combination with the triple-ζ quality TZVP[6] basis set on Co, O, N, and selected C atoms, and double ζ quality split-valence basis set, def2-SVP[7] on the rest of the atoms (B1 basis set). The broken-symmetry formalism developed by Noodleman[8, 9] was employed to describe states involving antiferromagnetic coupling. The following thresholds were used for optimizations: energy change tolerance of 5 × 10^{-6} a.u., root mean square gradient of 1 × 10^{-4} a.u., maximum gradient of 3 × 10^{-4} a.u., root mean square displacement of 2 × 10^{-3} a.u., maximum displacement of 4 × 10^{-3} a.u. The DFT integration grid was always set to Grid6 while the Hartree Fock exchange was evaluated by GridX6 for calculations with the B3LYP functional. Tight convergence criteria (energy tolerance 1 × 10^{-8} a.u.) for self-consistent field (SCF) calculations were employed throughout all calculations. The atom-pairwise dispersion correction with Becke-Johnson damping (D3BJ), as implemented in ORCA[10, 11] was used throughout to treat non-covalent interactions. The resolution of identity (RI) approximation[12-14] was used to accelerate the calculations in conjunction with the auxiliary Coulomb-fitting basis set def2/J to accelerate

the calculations at the BP86 level. To account for relativistic effects, scalar relativistic zeroth order approximation (ZORA) was used.[15-18] Geometry optimizations were performed without any constraints. Solvent effects during optimization and single point calculations were modeled by employing the polarizable continuum model (CPCM)[19] using benzene (ε = 2.3) as the solvent. Harmonic vibrational analyses were undertaken after the geometry optimization of each structure to differentiate local minima from transition states. The local minima were characterized by all positive eigenvalues of the Hessian matrix, whereas the transition states (TSs) have only one negative eigenvalue. The zero-point energies (ZPE), enthalpic corrections and entropic contributions were obtained from the frequency calculations. In order to obtain single-point energies closer to the basis set limit, B3LYP[4, 20] and M06L[21] calculations with the larger def2-TZVPP[22] basis set on all elements were carried out for which the auxiliary basis set def2-TZVPP/J was employed for the RIJCOSX or RI approximation as appropriate.[23] Empirical dispersion correction[24, 25] with the D3BJ keyword was employed all throughout except for calculations with M06L. The BP86 calculations on **TS4** and **11** (at S = 0) leads to an erroneous change in the local spin state of the two cobalt centers, deviating from the desired electronic structure. Since both species are involved in the rate-determining step of the dinuclear dissociative pathway, we re-optimized them (at S = 0 and 3 spin states) at the B3LYP/B1 level of theory. To be consistent, we optimized structures corresponding to rate-determining transition states and the reference intermediates/adducts among various pathways (such as **5, TS2, 6, 10, TS4, 11, 13, 14,** and **TS7)** at B3LYP/B1 and evaluated single point energies at M06L/def2-TZVPP. Reported relative free energies in this work are calculated at the M06L/def2-TZVPP level of theory unless otherwise mentioned. Finally, highly accurate electronic energies were computed by using open-shell DLPNO-CCSD(T)[26, 27] approach in conjunction with the def2-TZVPP basis set and an additional correlation fitting auxiliary basis set, def2-TZVPP/C. For pair natural orbital (PNO)

generation, the default values of *TCutPNO*, *TCutPairs* and *TCutMKN* were used.[28] Localized orbitals according to the Pipek-Mezey scheme were computed before PNO generation. Solvent corrections to coupled-cluster electronic energies were obtained from the M06L calculations. Due to the challenging computational cost, only crucial barriers were computed with coupled-cluster theory and the rest with M06L/def2-TZVPP. The gas phase Gibbs free energy change on addition/binding of CO_2 was corrected to the standard state (1 M) by using a correction factor of 1.89 kcal/mol.[29] This value is added to the relative free energy, when one molecule of CO_2 interacts with the mononuclear or dinuclear metal complexes to form the corresponding CO_2 adducts, which requires transfer of CO_2 from the gas phase into benzene solution.

To determine the electronic structure of **3**, we employed the multi-reference CASSCF[30, 31] approach.[32] The crystal structure of **3** was used as a starting point for geometry optimization, and to reduce computational cost, the two *tert*-butyl groups in the ligand were replaced with methyl groups. Geometry optimizations were performed using the BP86 functional and the B1 basis set combination. This approximation does not alter the electronic structure of the Co-O-Co moiety. The state-specific CASSCF (in the singlet spin state) calculations employed the triple-ζ quality def2-TZVPP basis set for all atoms with optimization of the first root. The active space consists of all 3d orbitals of both cobalt centers and the 2p orbitals of the bridging oxo ligand, which results in the active space CASSCF(20,13), 20 electrons distributed into 13 orbitals. Furthermore, to explore the effects of electronic excitations from filled π to vacant π* orbitals of the ligand, larger active spaces were constructed including the bonding and antibonding π-orbitals of the N-C-C-C-N of the β-diketiminate framework. This active space constituted of 24 electrons in 17 orbitals (CASSCF(24,17)). To make the computation of CASSCF(24,17) faster, the configuration interaction here has been treated with the ACCCI approximation.

B. ^{1}H NMR spectra

Figure S1. ^{1}H NMR spectrum of **3** in C_6D_6 at 25 °C.

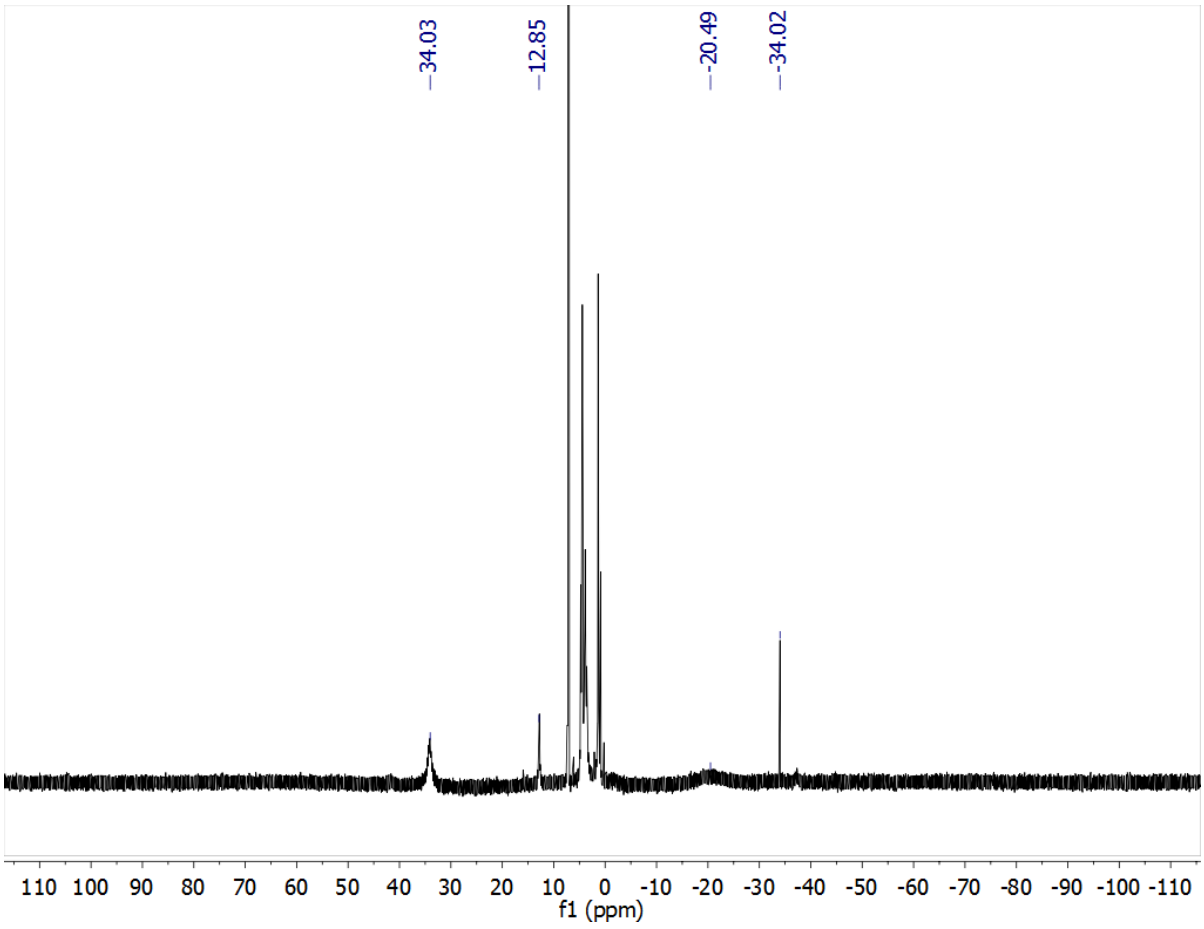

Figure S2. ^{1}H NMR spectrum of **4** in C_6D_6 at 25 °C.

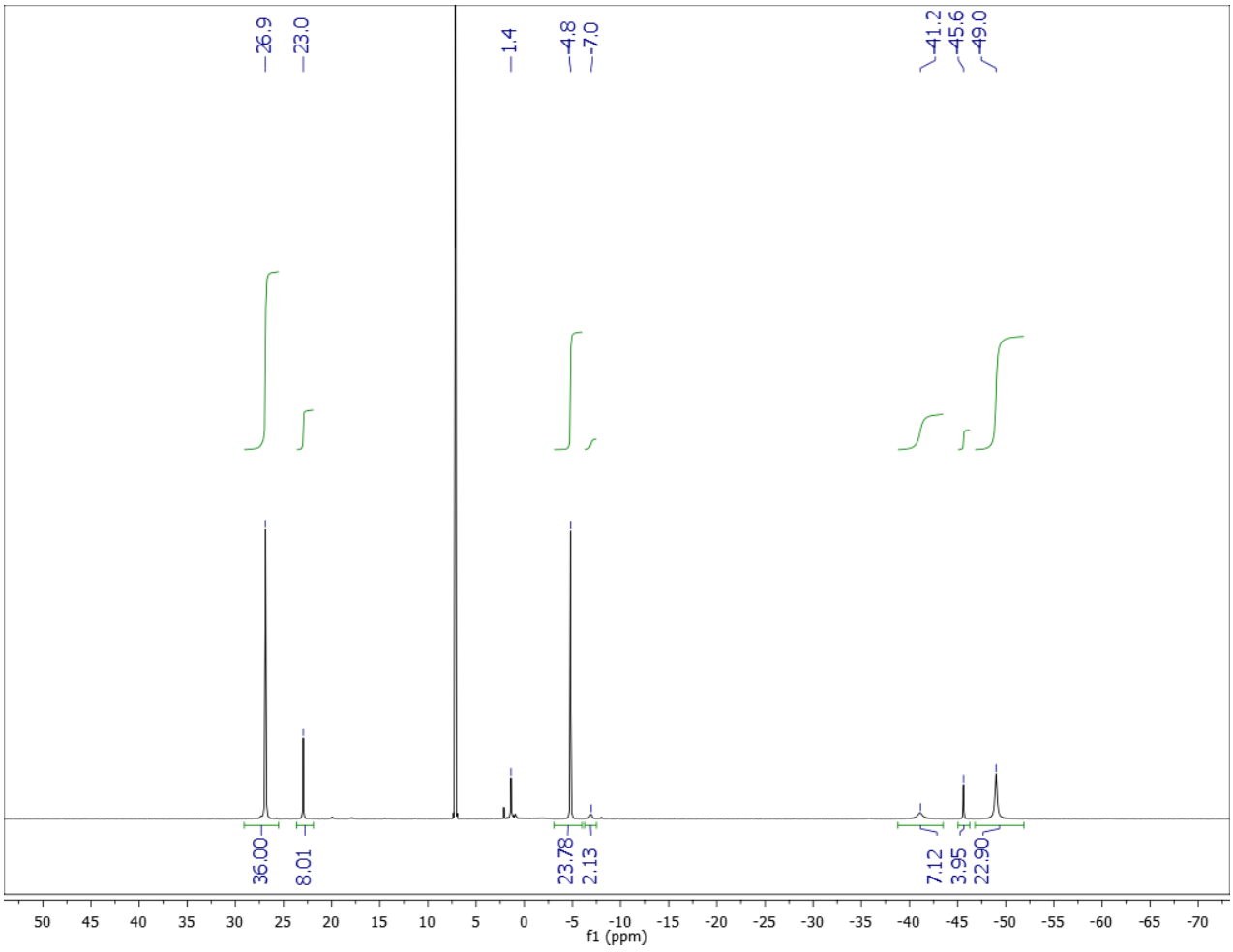

Figure S3. ^{1}H NMR spectra of reaction mixture of $L^{tBu}Co$ (**1**) with 10 equiv CO_2 monitored over time at 10 °C in C_6D_{12}. Integration with respect to a nickelocene internal standard shows that $L^{tBu}Co(CO)$ (**2**) is made in 95% spectroscopic and $L^{tBu}Co(OCO_2)CoL^{tBu}$ (**4**) is made in 86% spectroscopic yield after 3 h.

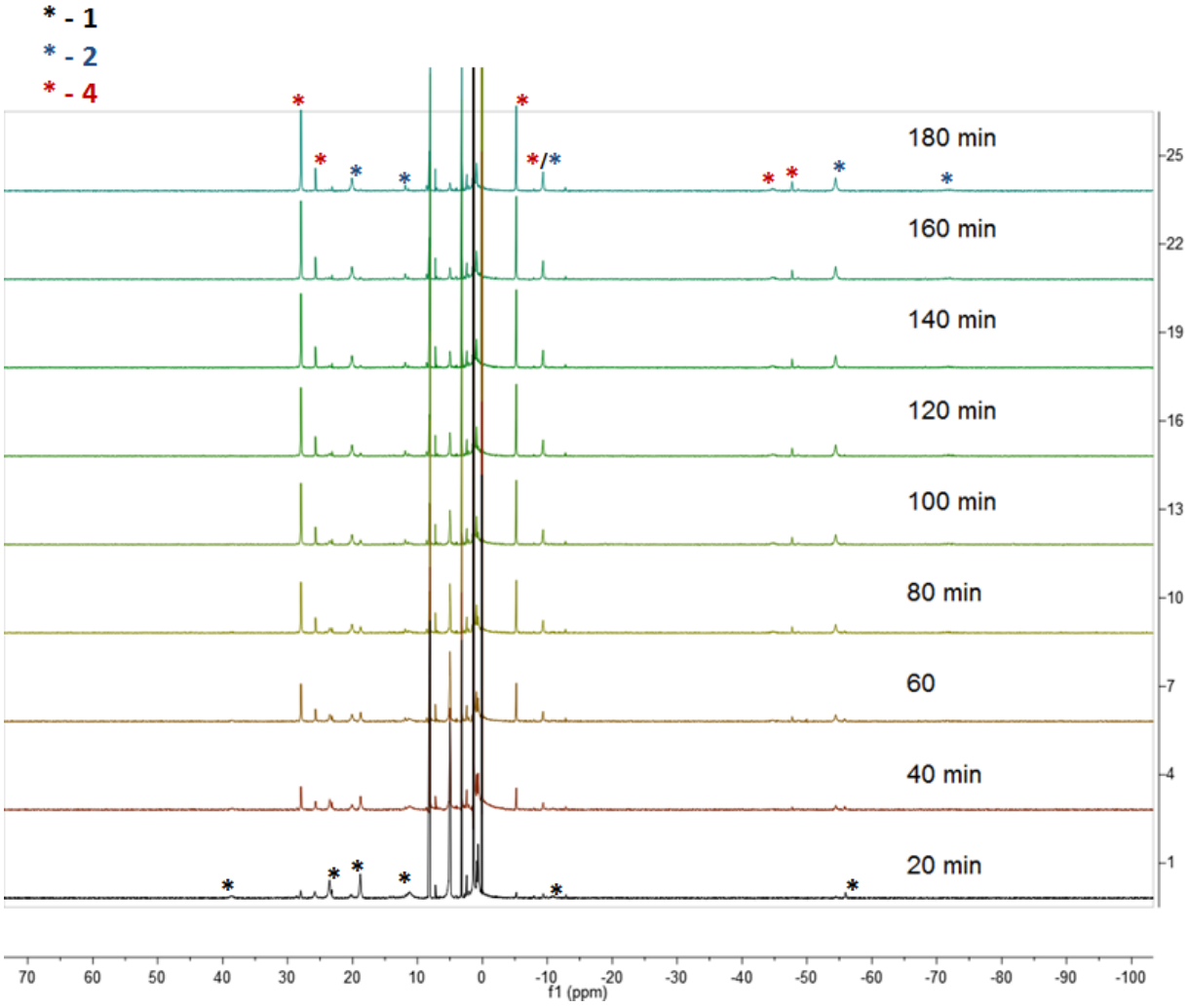

Figure S4. ^{1}H NMR spectrum (25 °C) of crude product mixture from reaction of $L^{tBu}Co$ with 10 equiv of CO_2 in C_6D_{12}.

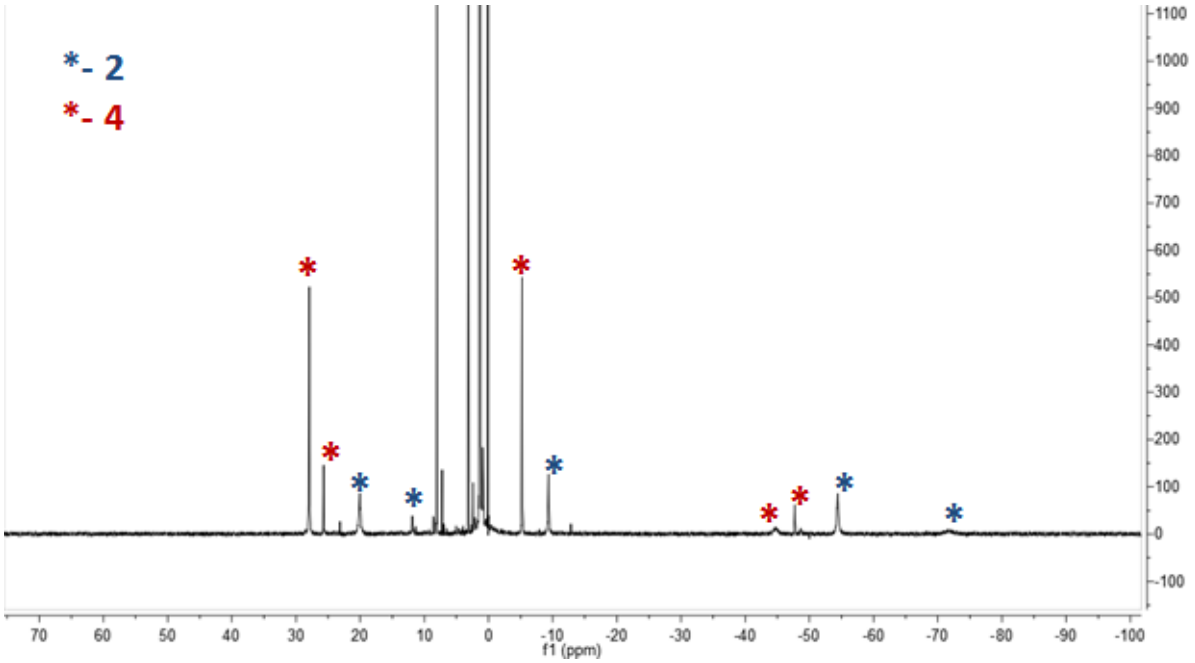

Figure S5. ^{1}H NMR spectra of a reaction mixture of **3** before (below) and 2 min after (above) adding 1.5 equiv of CO_2 at 10 °C in C_6D_{12}. Integration relative to a nickelocene internal standard indicates formation of **4** in 75% spectroscopic yield.

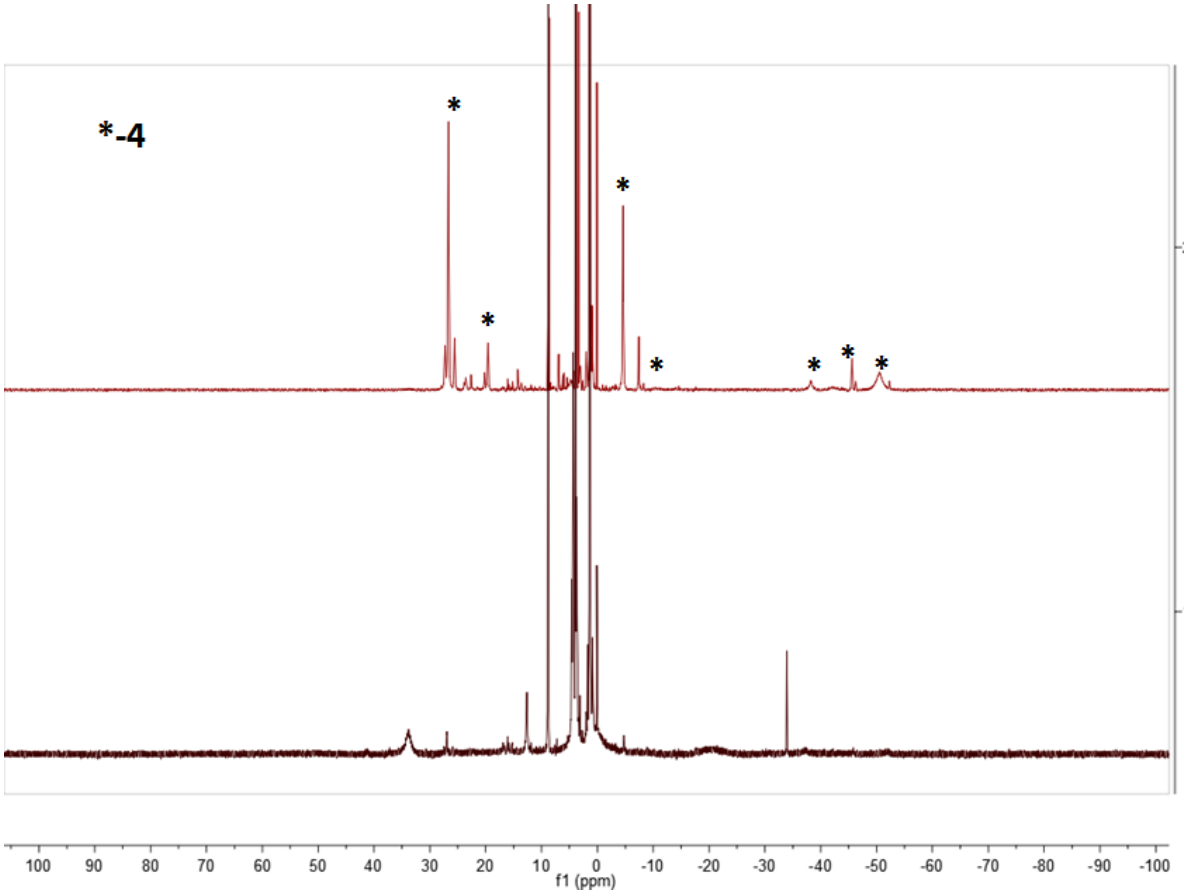

C. NMR kinetics of CO_2 reduction by $L^{tBu}Co$.

A general procedure for one flooding concentration of CO_2 is described. Under an Ar atmosphere, a stock solution of **1** in C_6D_{12} (0.200 mL, 13.4 mM, 0.00268 mmol), 0.400 mL of C_6D_{12}, and a nickelocene capillary integration standard were added to a J. Young NMR tube. The NMR tube was sealed with a rubber septum and the solution was flash frozen in a liquid N_2 bath. A stock solution of CO_2 in C_6D_{12} (0.400 mL, 72.9 mM, 0.0292 mmol) was injected anaerobically by syringe. The solution was thawed and injected into an NMR spectrometer pre-cooled to 10 °C. Proton NMR spectra were acquired at 10°C every 10 min for 5 h.

This general procedure was followed to measure two different flooding concentrations of CO_2 as well as two initial concentrations of **1** as indicated below. The concentration over time profiles of $L^{tBu}Co$ (**1**), $L^{tBu}Co(CO)$ (**2**), and $L^{tBu}Co(\mu\text{-}OCO_2)CoL^{tBu}$ (**4**), as determined by integration of proton NMR data, were fit to first-order kinetics for each run. The value of the rate constant *k* for each run was then calculated as the average of the three observed rate constants obtained for a given experiment. Using these rate constants in the Eyring equation, a value of $\Delta G^{\ddagger}$=21.0 kcal/mol is obtained.

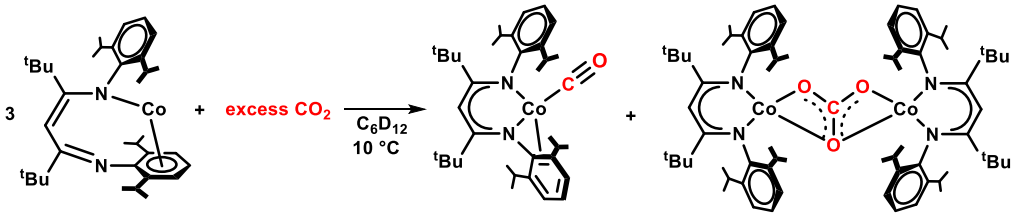

Kinetics Conditions

- **Run 1:** [LCo] = 2.67 mM, [CO_2] = 29.2 mM
- **Run 2:** [LCo] = 2.67 mM, [CO_2] = 58.4 mM
- **Run 3:** [LCo] = 5.34 mM, [CO_2] = 29.2 mM

	LCo fit (k*10^4 s^{-1})	LCo(CO) fit (k*10^4 s^{-1})	LCo(OCO)CoL fit (k*10^4 s^{-1})	Average (k*10^4 s^{-1})
Run 1	4.21	3.65	3.86	3.91
Run 2	3.79	3.81	3.55	3.72
Run 3	3.21	3.38	3.74	3.44

Figure S6. Reactant and product concentration over time data as determined by NMR spectroscopy in C_6D_{12} at 10 °C; data and first-order fits correspond to Run 1 above.

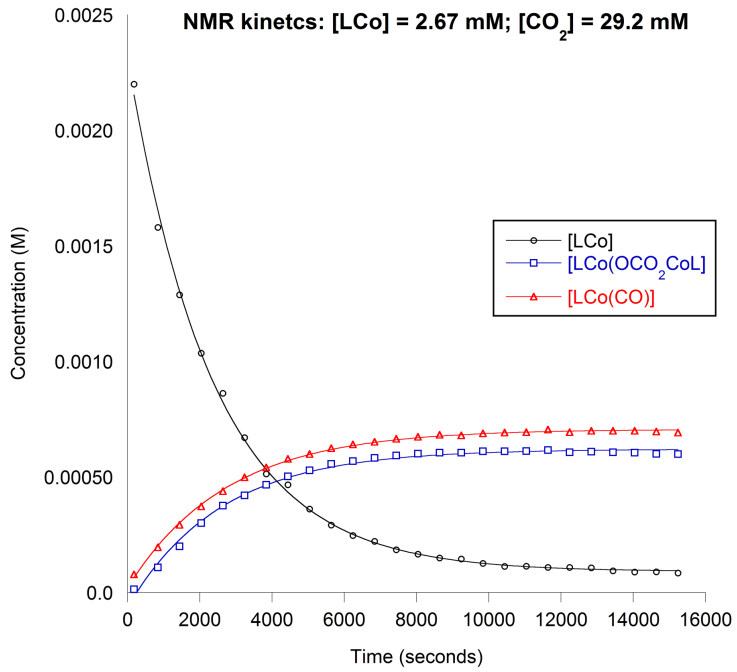

y = m2*exp(-k*x)+m1		
	Value	Error
m1	0.00070648	2.1242e-6
m2	-0.00068437	5.519e-6
k	0.0003651	6.0158e-6
Chisq	8.8748e-10	NA
R	0.9994	NA

y = m2*exp(-k*x)+m1		
	Value	Error
m1	0.00062019	4.3928e-6
m2	-0.00068194	1.2214e-5
k	0.00038628	1.3754e-5
Chisq	4.1404e-9	NA
R	0.9971	NA

y = m2*exp(-k*x)+m1		
	Value	Error
m1	9.1137e-5	6.8343e-6
m2	0.0022242	2.0918e-5
k	0.00042071	7.5843e-6
Chisq	1.1281e-8	NA
R	0.99922	NA

Figure S7. Reactant and product concentration over time as determined by NMR spectroscopy in C_6D_{12} at 10 °C; data and first-order fits correspond to Run 2 above.

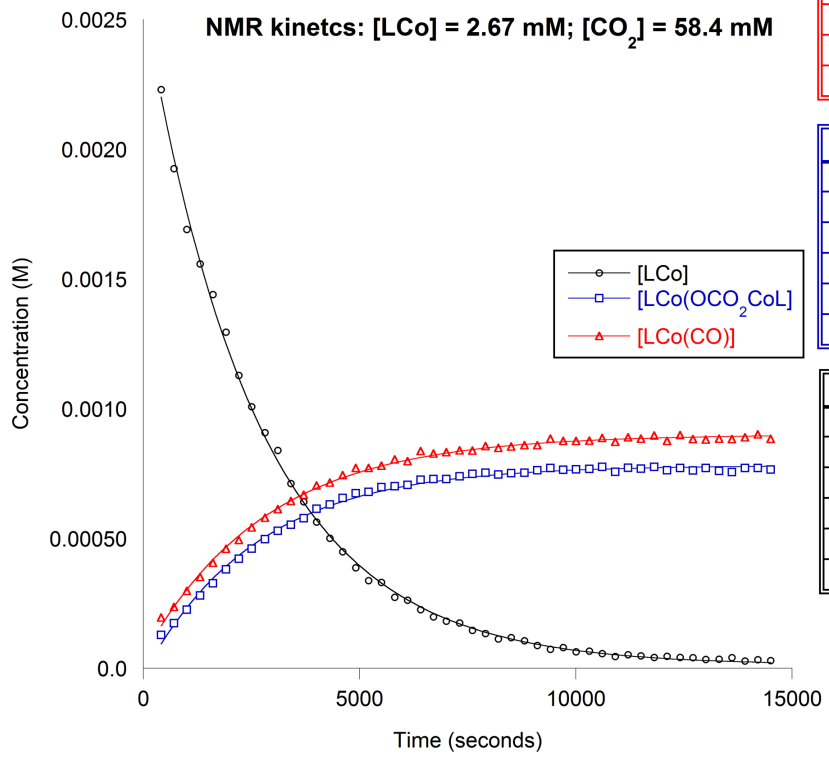

y = -m2*exp(-m3*x)+m1		
	Value	Error
m1	0.00090046	2.8547e-6
m2	0.00085283	8.1673e-6
m3	0.00035507	6.5649e-6
Chisq	4.7767e-9	NA
R	0.99863	NA

y = -m2*exp(-m3*x)+m1		
	Value	Error
m1	0.00078188	2.9368e-6
m2	0.00080499	9.4261e-6
m3	0.00038146	8.1828e-6
Chisq	5.7463e-9	NA
R	0.99806	NA

y = m2*exp(-m3*x)+m1		
	Value	Error
m1	1.176e-5	4.9298e-6
m2	0.0025576	1.5671e-5
m3	0.00037911	4.2737e-6
Chisq	1.6022e-8	NA
R	0.99947	NA

Figure S8. Reactant and product concentration over time as determined by NMR spectroscopy in C_6D_{12} at 10 °C; data and first-order fits correspond to Run 3 above.

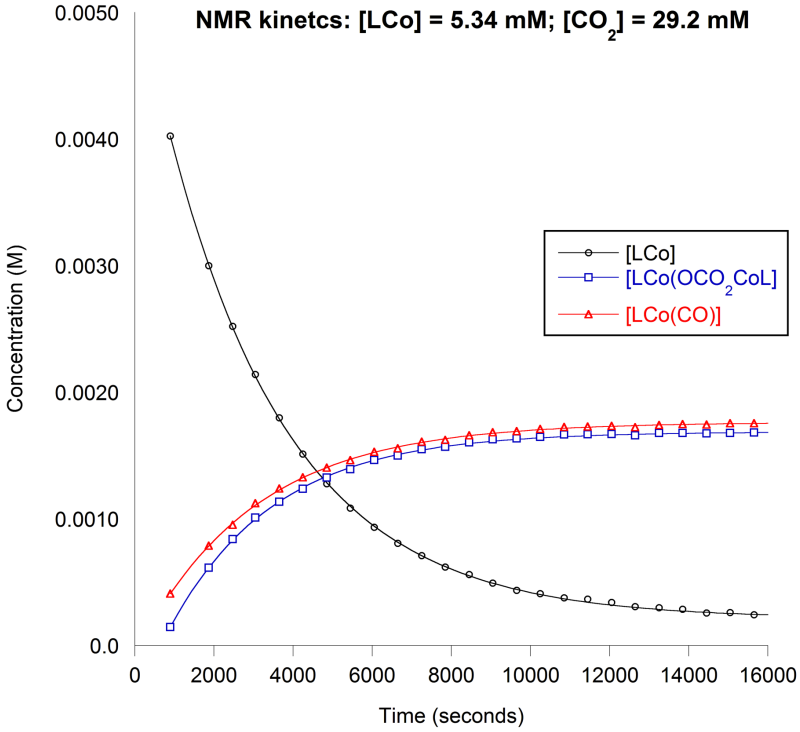

y = m2*exp(-m3*x)+m1		
	Value	Error
m1	0.00021326	2.6787e-6
m2	0.0050861	1.6162e-5
m3	0.00032073	1.2914e-6
Chisq	7.4237e-9	NA
R	0.99988	NA

y = -m2*exp(-m3*x)+m1		
	Value	Error
m1	0.0017634	1.4222e-6
m2	0.001834	9.3184e-6
m3	0.00033761	2.1087e-6
Chisq	2.2643e-9	NA
R	0.9997	NA

y = -m2*exp(-m3*x)+m1		
	Value	Error
m1	0.0016877	1.8803e-6
m2	0.0021566	1.4427e-5
m3	0.00037393	2.9169e-6
Chisq	4.5503e-9	NA
R	0.99951	NA

D. Attempted synthesis of CO coordinated oxo complex 11

General procedure for CO gas addition to complex 3: Solid **3** (2.7 mg, 0.0023 mmol) was dissolved in 0.6 mL benzene-d_6 and transferred to a J. Young NMR tube containing a nickelocene capillary used as an integration standard. On the Schlenk line, the NMR sample solution was frozen using a liquid nitrogen cold bath. The headspace above the frozen solution was evacuated. CO (7 mbar, 12.55 mL, 0.0035 mmol) was condensed on the frozen solution for 20 min and then the NMR sample was sealed and thawed to ambient temperature with vigorous shaking. Proton NMR indicated formation of the known cobalt bis(carbonyl) complex $L^{tBu}Co(CO)_2$[3] in 34% spectroscopic yield in addition to unidentified minor species.

Figure S9. Proton NMR spectra of reactions between **3** and CO.

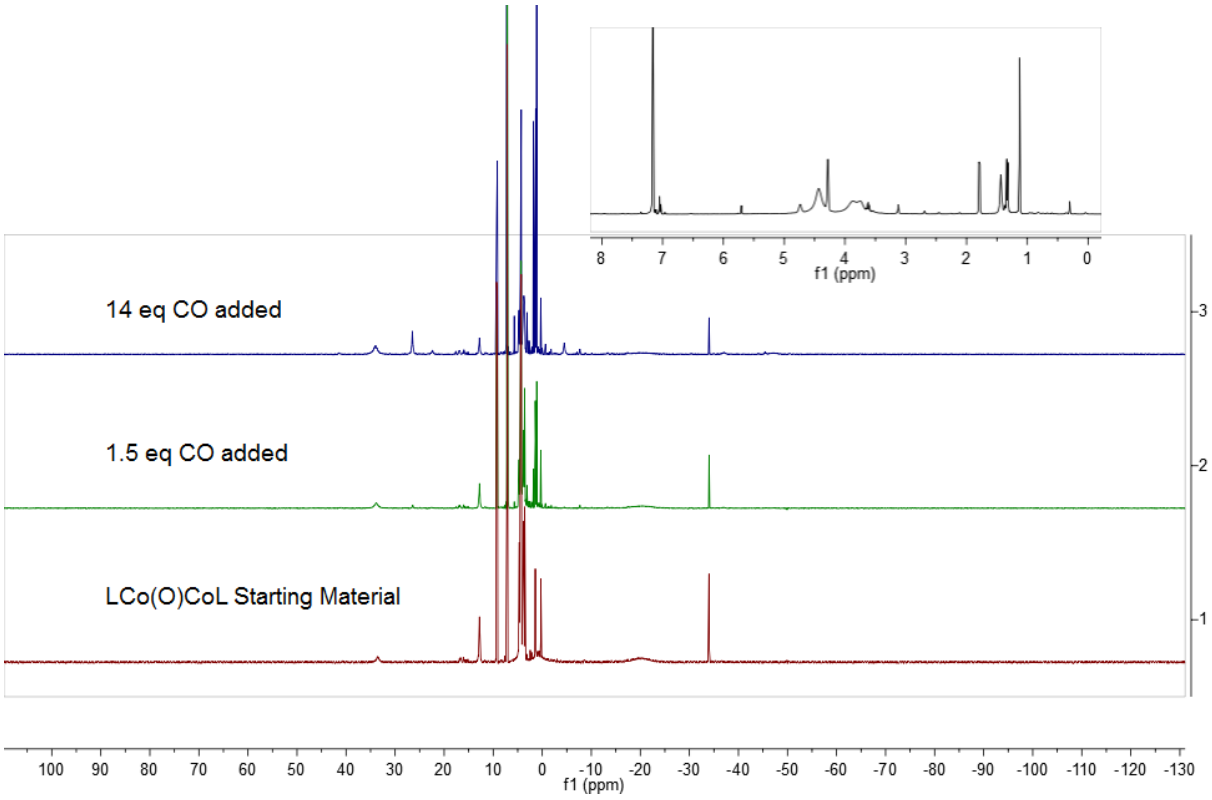

E. X-ray absorbance spectroscopy of $L^{tBu}Co(O)CoL^{tBu}$ (3) and reference compounds

High Energy Resolution Fluorescence Detection X-ray Absorption Spectroscopy (HERFD-XAS) data were collected at the Cornell High Energy Synchrotron Source at C-line end station. The incident X-rays were monochromated using a Si(220) crystal monochromator. Emitted X-rays were analyzed using a set of three spherically bent Si crystals (531 reflection) mounted on a Rowland circle in combination with a Pilatus Area Detector as previously described.[33, 34] He-filled plastic bags were used to displace air from the beam flight path to minimize attenuation of the fluorescence. The Co HERFD-XAS spectra were collected by monitoring the intensity of the $K\alpha_1$ peak as a function of incident energy. Data were collected from 7650 to 7950 eV. A step size and count time of 10 eV (1 sec), 0.3 eV (5 sec), and 2 eV (2 sec) was used from 7650 to 7690 eV, 7690 to 7750 eV and 7750 to 7950 eV respectively. Data were collected at *ca.* 20 K in a Displex cryostat to minimize photoreduction and to maintain the samples in an inert atmosphere. The data were normalized using PyMCA and six experimental spectra were averaged for each compound. For normalization, the postedge region (E > 7750 eV) was set to an absorbance of 1.0. The first inflection point of Co foil was used as a calibrant, adjusting the energy axis to the reported literature value of 7709.5 eV. All samples were prepared in a nitrogen filled glovebox as 5% Co (wt/wt) solid dilutions in BN.

Figure S10. Cobalt K-edge X-ray absorbance spectra of $L^{tBu}Co(O)CoL^{tBu}$ (**3**) and cobalt(II) (LCoCl, three-coordinate; $[LCo(OH)]_2$, four-coordinate) and cobalt(III) ($[LCo(O)]_2$, four-coordinate) reference compounds. The method of preparation for the last two compounds was recently described.[35]

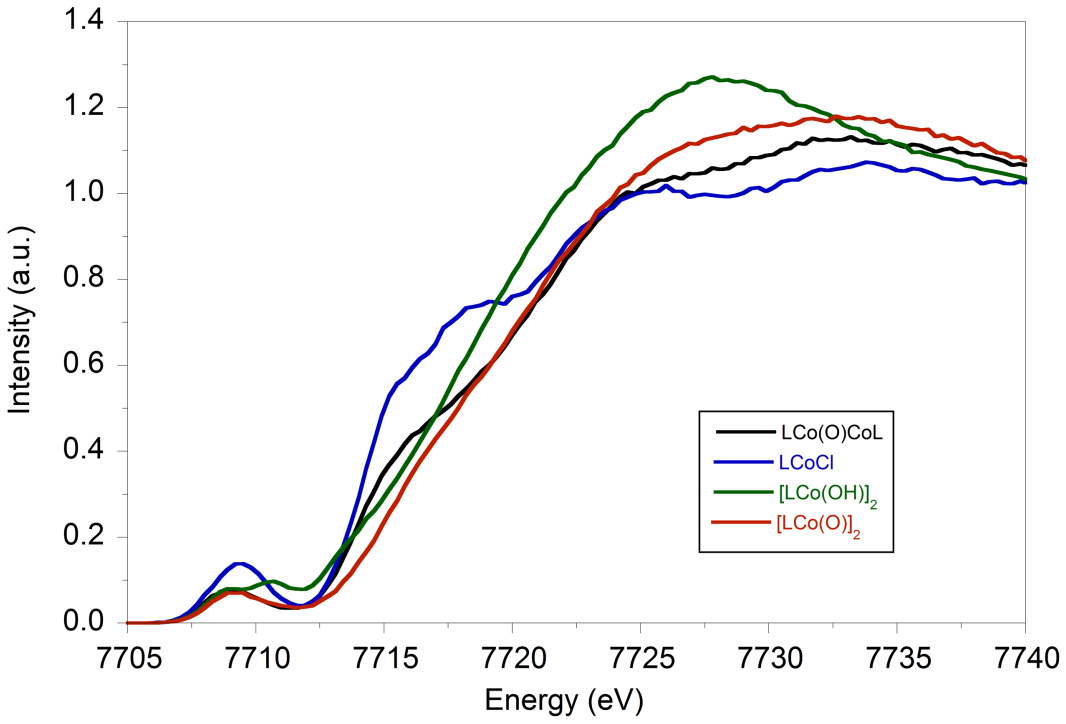

F. X-ray crystallography

Crystals were placed onto the tip of a 0.1 mm diameter glass capillary tube or fiber and mounted on a Bruker SMART APEX II CCD Platform diffractometer for a data collection at 100.0(5) K.[1] The full data collection was carried out using MoKα radiation (graphite monochromator). A randomly oriented region of reciprocal space was surveyed: six major sections of frames were collected with 0.50° steps in ω at six different ϕ settings and a detector position of -38° in 2θ. The intensity data were corrected for absorption.[2] Final cell constants were calculated from the xyz centroids of >3800 strong reflections from the actual data collection after integration.[3]

Structure (**3**) was solved using SIR97[4] and refined using SHELXL-2012.[5] The space group P-1 was determined based on intensity statistics. A direct-methods solution was calculated which provided most non-hydrogen atoms from the E-map. Full-matrix least squares / difference Fourier cycles were performed which located the remaining non-hydrogen atoms. All non-hydrogen atoms were refined with anisotropic displacement parameters. All hydrogen atoms were placed in ideal positions and refined as riding atoms with relative isotropic displacement parameters. The structure suffered both from non-merohedral twinning and highly disordered solvent. After the non-merohedral twin law, [-0.510 0.497 -0.020 / 1.470 0.490 -0.061 / -0.490 -0.497 -0.980], a 180 degree rotation about reciprocal lattice [-1 -3 1], was determined,[6] the data were re-integrated,[3] and a new absorption correction was applied. There were 21623 unique reflections solely in the first component, 21604 unique reflections solely in the second component, and 4867 unique overlapping reflections. The mass ratio of the two components refined to 60:40. However, since the structure also contained highly disordered solvent (toluene and perhaps hexane), the overlapping reflection contributions from the minor mass component of the twin were removed.[7] Once the data were modified for twinning, they were further modified to remove reflection contributions from the disordered solvent.[8] There were 4 sites of ~200 Å^3 each in which around 75 electrons were removed, for a total of 297 electrons in 829 Å^3 removed per unit cell. Since the exact amount and identity of solvent were unknown, no solvent was included in the atom list or molecular formula.

Structure (**4**) was solved using SIR97[4] and refined using SHELXL-97.[9] The space group Cc was determined based on systematic absences and intensity statistics. A direct-methods solution was calculated which provided most non-hydrogen atoms from the E-map. Full-matrix least squares / difference Fourier cycles were performed which located the remaining non-hydrogen atoms. All non-hydrogen atoms were refined with anisotropic displacement parameters. All hydrogen atoms were placed in ideal positions and refined as riding atoms with relative isotropic displacement parameters. The structure was refined as an inversion twin, with a final twin occupancy ratio of 87:13.

Table S1. Crystallography of **3** and **4**

Complex	**3**	**4**
Empirical formula	$C_{70}H_{106}Co_2N_4O$	$C_{71}H_{106}Co_2N_4O_3$
FW	1137.44	1181.46
Crystal system	Triclinic	Monoclinic
Space group	P-1	Cc
a (Å)	13.475(2)	20.919(2)
b (Å)	21.712(2)	28.234(3)
c (Å)	25.061(3)	24.420(3)
α (deg)	95.195(3)	90
β (deg)	102.214(2)	114.237(2)
γ (deg)	97.097(3)	90
V (Å^3)	7060(1)	13152(3)
Z	4	8
ρ (g/cm^3)	1.070	1.193
μ (mm^{-1})	0.510	0.552
***R*1, *wR*2 (I > 2σ(I))**	0.0745, 0.1714	0.0603, 0.1053
***R*1, *wR*2 (all data)**	0.1348, 0.1960	0.1182, 0.1260
GOF	0.918	0.973

Crystallographic References

1. *APEX2*, version 2012.4-3; Bruker AXS: Madison, WI, 2012.
2. Sheldrick, G. M. *SADABS*, version 2008/1; University of Göttingen: Göttingen, Germany, 2008.
3. *SAINT*, version 7.68A; Bruker AXS: Madison, WI, 2009.
4. Altomare, A.; Burla, M. C.; Camalli, M.; Cascarano, G. L.; Giacovazzo, C.; Guagliardi, A.; Moliterni, A. G. G.; Polidori, G.; Spagna, R. *SIR97: A new program for solving and refining crystal structures*; Istituto di Cristallografia, CNR: Bari, Italy, 1999.
5. Sheldrick, G. M. *SHELXL-2012* University of Göttingen: Göttingen, Germany, 2012.
6. a) Parsons, S.; Gould, B.; Cooper, R.; Farrugia, L. *ROTAX*; University of Edinburgh: Edinburgh, Scotland, 2003; b) Sheldrick, G. M. *CELL_NOW: A program that analyzes a list of reflections to find a cell and orientation matrix despite the presence of several twin domains or other junk*, version 2008/2; University of Göttingen: Göttingen, Germany, 2008.
7. Sheldrick, G. M. *TWINABS*, version 2008/4; University of Göttingen: Göttingen, Germany, 2008.
8. Spek, A. L. *PLATON: A multipurpose crystallographic tool*, version 300106; Utrecht University: Utrecht, The Netherlands, 2006.
9. Sheldrick, G. M. *Acta*. *Cryst*. **2008**, *64*, 112-122.

G. Justification for truncating the computational ligand model

Figure S11. Overlay of the optimized geometry of $L^{tBu}Co$ and L'Co with the crystal structure calculated at BP86/B1 with D3BJ correction (see below for basis set information)**.**

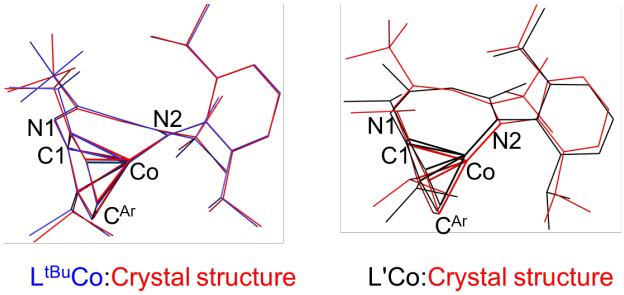

Table S2. Crystallographically obtained and DFT calculated interatomic distances (Å) and angles (°) for $L^{tBu}Co$ and L'Co. Deviations from crystal structure are shown by Δ and written in parenthesis.

	Crystal Structure	**$L^{tBu}Co$ (Δ)**	**L'Co (Δ)**
Co-N1	3.16	3.16 (0.0)	3.19 (0.03)
Co-C1	2.09	2.08 (-0.01)	2.09 (0.0)
Co-C^{Ar}	2.15	2.16 (0.01)	2.12 (-0.03)
Co-N1-C1	30.8	30.3 (-0.5)	29.0 (-1.8)
Co-N2	1.90	1.88 (-0.02)	1.87 (-0.03)

Comparing the geometrical parameters of $L^{tBu}Co$ and L'Co (Table S2) obtained at BP86(D3BJ)/B1 level of theory (B1 basis set includes TZVP basis employed on Co and N and def2-SVP basis on C and H atoms) and an overlay of their geometries with the actual crystal structure (Figure S11) show quite good agreement among all the three structures. The bond lengths and angles of the optimized geometries of the model complexes are consistent with the X-ray crystal structure with insignificant deviations (shown in Table S2). This also validates the reliability of the method chosen for optimization. Moreover, the κ-*N*,η^6-arene ligation is well reproduced in the initial geometry of the complex, i.e. L'Co. The ^{t}Bu substituents on the crystal structure and the methyl replacers in L'Co are almost collinear. This justifies the validity of the truncated model L'Co to be used in place of the actual $L^{tBu}Co$ framework. However, whenever necessary, the original $L^{tBu}Co$ framework has been used for calculations; for example in comparing the calculated and experimental structure for dinuclear carbonate (shown in Table 1, main text) and also for μ-oxo dicobalt species (shown in Table 2, main text).

H. Benchmarking the various density functional methods with DLPNO-CCSD(T).

It is observed from Figure S12 that single point energy calculations on optimized geometries (optimized at BP86(D3BJ)/B1) along the reaction coordinate leading to transformation of **1** to **1'** followed by CO_2 addition shows variations in the relative barriers depending on the choice of wavefunction based method and density functional. In particular, it is found that B3LYP with and without empirical dispersion correction deviates from the DLPNO-CCSD(T) predicted relative free energies. B3LYP functional predicted that the C-O bond cleavage in the dinuclear dissociative pathway via **TS4** is the rate determining step. However, it would indicate a buildup of the dinuclear carboxylate bridging intermediate **10**, in contrast to the observed reaction. Repeated experimental attempts could not observe the κ^2*N,N'* isomer (**1'**) of the starting material **1** which indicates that the RDS should be the ligand isomerization. Also kinetics studies showed that the rate does not depend on the concentration of CO_2 (as has been discussed in section C of this supporting information), which further emphasized on the experimental identification of only the κ*N,*η^6-arene isomer. B3LYP on the other hand underestimated the metal-aryl bonding and predicted the κ^2N,N' isomer to be lower in energy by -10 kcal/mol than the κN,η^6-arene isomer, in disagreement to the experiments (see Figure S12). Interestingly, M06L/def-TZVPP delivers a similar barrier for **TS1** as DLPNO-CCSD(T)/def2-TZVPP. This observation suggests that the B3LYP functional even with the non-covalent corrections cannot properly describe the metal aryl π-bonding in κ-*N,*η^6-arene ligated L'Co, whereas M06L is designed to cover the weak interactions. Hence based on this observation, we predict all the important barriers and reaction free energies with DLPNO-CCSD(T)/def2-TZVPP and M06L/def2-TZVPP in the main text.

Figure S12. Gibbs free energy (ΔG) profile for isomerization of **1** (L'Co) to **1'** followed by CO_2 activation at different levels of theory.

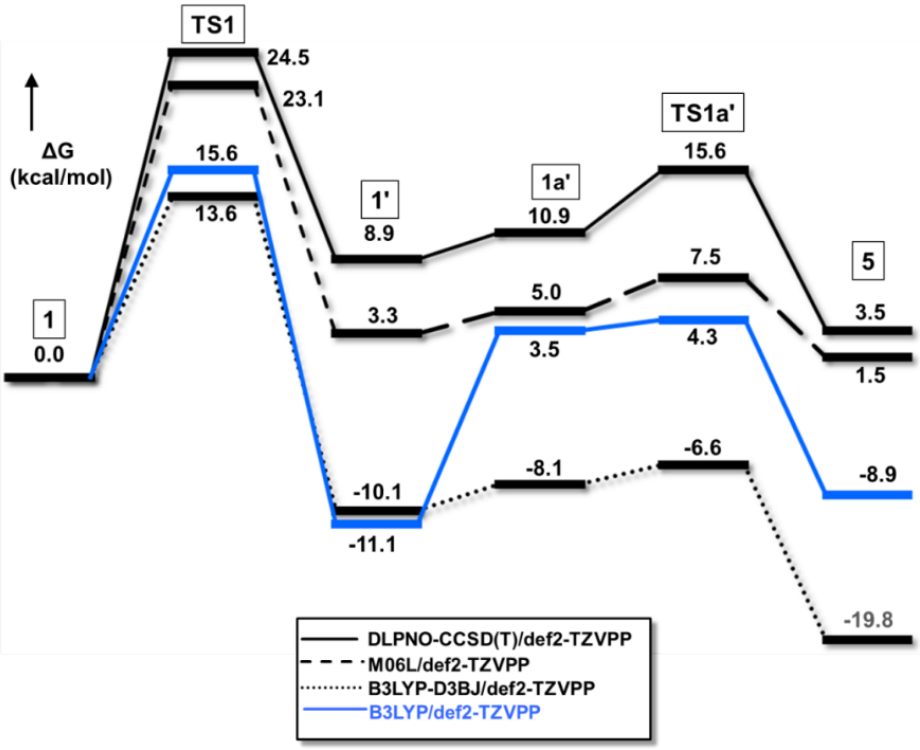

I. Different bridging binding modes of CO_2 with two metal complexes and their geometrical parameters.

Figure S13. The two different binding modes of bridging CO_2 possible with two metal complexes.

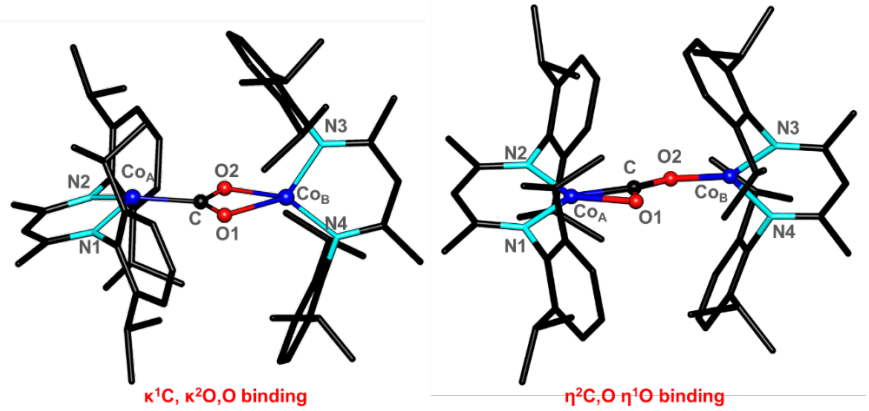

Table S3. Binding parameters and geometries of CO_2 bridged adducts. Distances in Å and angles in degrees.

η^1C, η^2O,O binding	Co_A-N1	Co_A-N2	Co_A-C	C-O1	C-O2	O1-C-O2	Co_B-O1	Co_B-O2	Co_B-N3	Co_B-N4
^{1}**10**$_{BS33}$	1.89	1.90	1.92	1.29	1.29	117.4	2.06	2.05	1.88	1.89
^{3}**10**$_{BS31}$	1.89	1.89	1.93	1.31	1.29	113.0	1.97	1.99	1.82	1.82
^{5}**10**$_{31}$	1.88	1.90	1.94	1.29	1.30	113.1	1.99	1.97	1.82	1.82
^{7}**10**	1.90	1.90	1.93	1.30	1.30	116.7	2.06	2.06	1.89	1.90
η^1C, η^2O,O binding										
^{1}**10**$_{BS11}$	1.88	1.83	1.81	1.30	1.28	125.0	2.84	1.91	1.78	1.80
^{3}**10**	1.88	1.83	1.81	1.30	1.28	125.2	2.86	1.91	1.78	1.80
^{3}**10**$_{BS13}$	1.88	1.83	1.81	1.33	1.27	119.0	2.14	2.05	1.89	1.89
^{5}**10**$_{13}$	1.88	1.83	1.81	1.33	1.27	119.2	2.14	2.03	1.89	1.89

The κ^1C, κ^2O,nding mode for the S=3 and S=0 (BS33) has been discussed in the main text.

J. Magneto-structural isomers of intermediate 10

Figure S14. The possible electronic structures of intermediate **10**. The overlap between non-orthogonal magnetic orbitals of broken symmetry UHF solution has been marked with the notation "S". The subscript represents the number of unpaired electrons locally on a center.

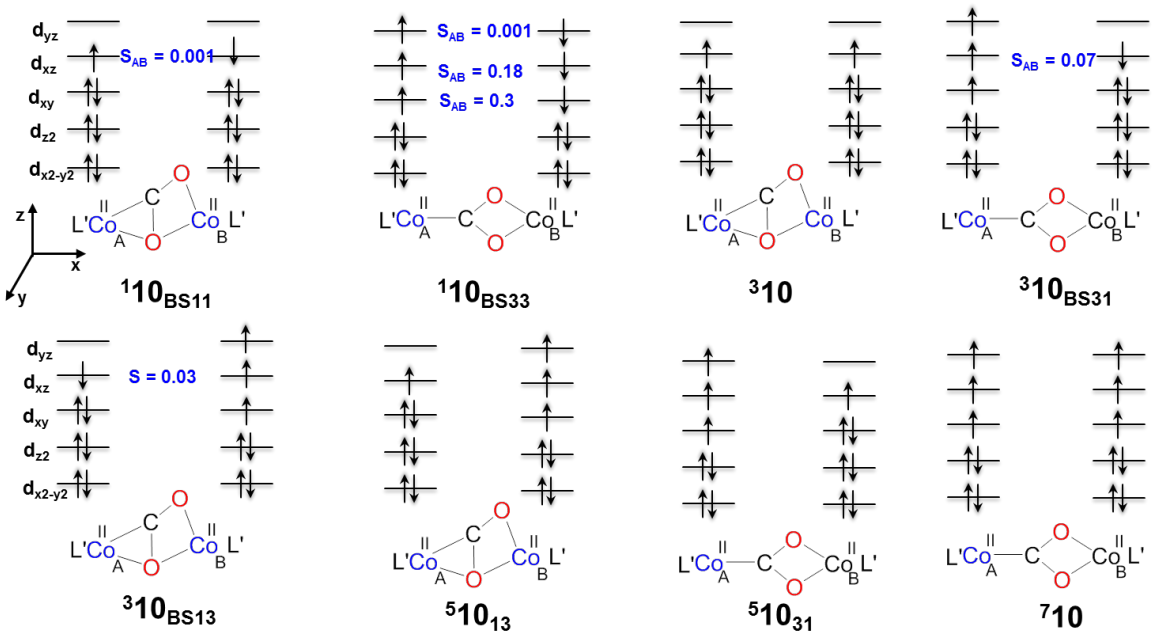

Table S4. Mulliken atomic spin population, total spin and free energy values as collected from B3LYP(D3BJ)/def2-TZVPP/B3LYP(D3BJ)/B1 calculations.

Intermediate	ϱCo_A	ϱCo_B	S	ΔG *(kcal mol^{-1})*
^{1}**10**$_{BS11}$	1.05	-1.03	0	19.1
^{1}**10**$_{BS33}$	2.60	-2.62	0	0.8
^{3}**10**	1.06	1.02	1	18.6
^{3}**10**$_{BS31}$	2.60	-1.0	1	7.4
^{3}**10**$_{BS13}$	-1.10	2.66	1	3.3
^{5}**10**$_{13}$	1.13	2.65	2	3.3
^{5}**10**$_{31}$	2.59	1.04	2	9.1
^{7}**10**	2.63	2.67	3	0.0

From Figure SI4 and Table S4 we find that the high spin septet intermediate with S=3/2 on both the cobalt (II) centers (^{7}**10**) possesses the same energy as the broken symmetry singlet, ^{1}**10**$_{BS33}$. Also, the ferromagnetically coupled quintet ^{5}**10**$_{13}$ and its corresponding antiferromagnetic triplet counterpart ^{3}**10**$_{BS13}$ have slightly higher energies than the high spin states. Hence, to reduce computational effort, we have chosen the lowest energy septet and the broken symmetry singlet to explore the reaction mechanism. It is to be noted that geometries of the chosen intermediate on these two states are also similar.

K. B3LYP calculated free energy profiles

Figure S15. B3LYP/def2-TZVPP Gibbs free energy (ΔG) profile for mononuclear (left) and dinuclear (right) dissociative pathway

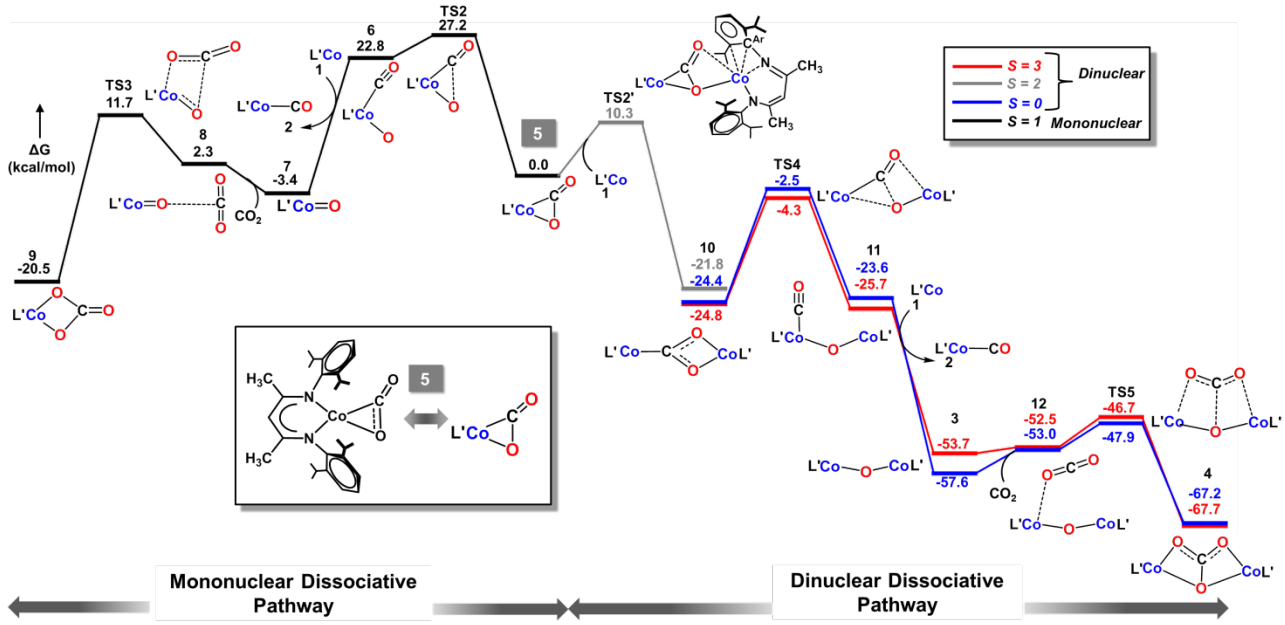

Figure S16. B3LYP/def2-TZVPP Gibbs free energy (ΔG) profile for dinuclear associative pathway.

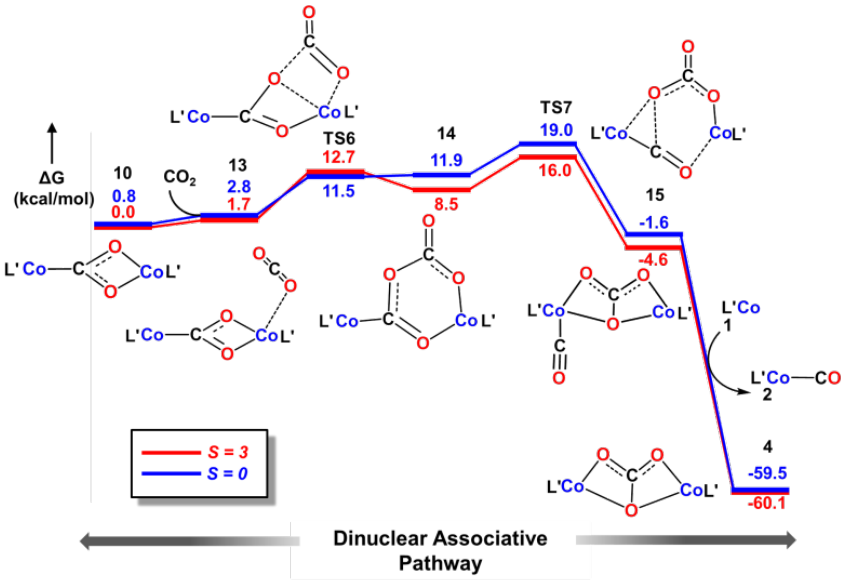

L. M06L calculated free energy profiles

Figure S17. M06L/def2-TZVPP Gibbs free energy (ΔG) profile for mononuclear and dinuclear dissociative and dinuclear associative pathways.

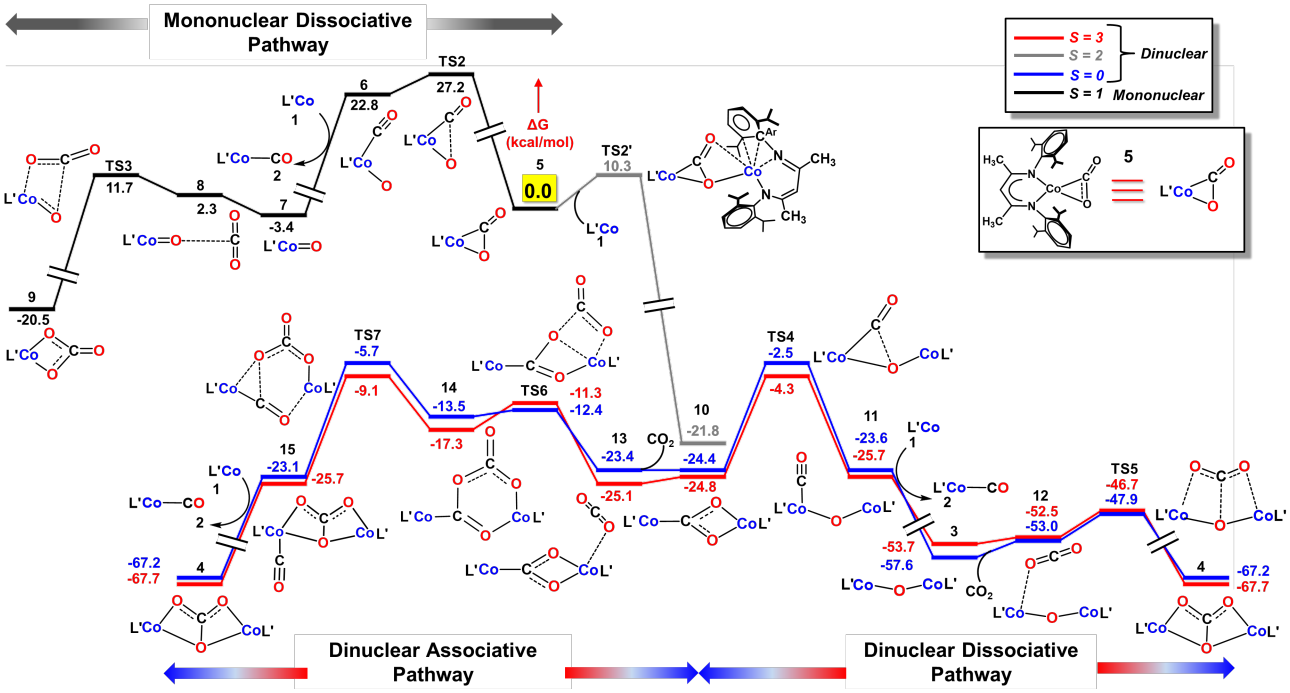

M. Optimized geometry of important intermediates and transition states with BP86/B1

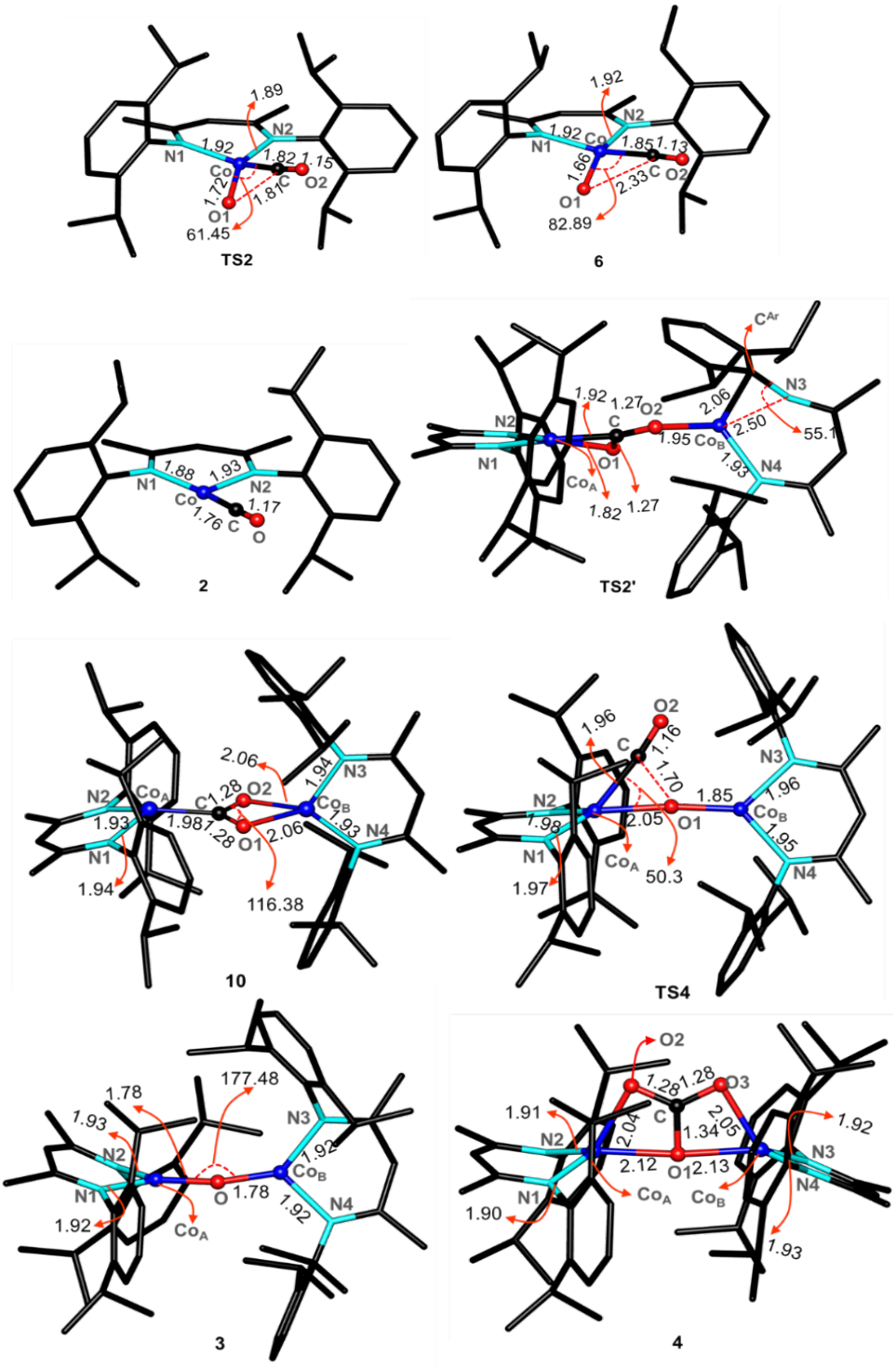

N. XYZ coordinates of optimized geometries.

$(L^{tBu}Co)_2\mu\text{-}CO_3$

Co	7.13217946770792	26.13376195867381	17.80263950116836
Co	9.99228411947636	22.70740819360404	17.81099296671146
C	7.79613357253401	23.77789028777456	18.18569685668649
O	6.63255194663147	24.29161534497207	18.36736510878959
O	8.75122954680276	24.56552223585289	17.72036234734129
O	8.09615756722283	22.55306062601858	18.42345691879625
N	6.82147517750987	27.58974709430260	19.03316992701278
N	6.51147324784066	26.90810352819571	16.14662318319071
C	4.91546147990525	29.14358748260706	19.83687196237873
C	5.75560022799669	28.37314062726186	18.75469583016602
C	5.21137265900650	28.44461420378086	17.45339207193712
H	4.35843895847155	29.11349082416984	17.38262333586399
C	5.59232290587258	27.88617688905426	16.20335057295230
C	4.87575558310163	28.56804422154542	14.98411154727617
C	5.56274869533388	29.36978320275432	21.22050536498660
H	4.80068234731106	29.83227144257115	21.87425225433752
H	6.42652297981954	30.05149180676707	21.17994021803052
H	5.89375383658315	28.44014346554600	21.70194549280776
C	3.65647605226582	28.25843255650254	20.05537047301396
H	2.99319819583949	28.72231256027773	20.80879792409150
H	3.94437003148302	27.25648035307819	20.42033339748997
H	3.08491266524602	28.12632193618841	19.12074156632291
C	4.48299872042992	30.54466527435017	19.33233680084662
H	3.95801006384418	31.07656109822108	20.14578798802812
H	3.79225450935474	30.51158802618719	18.47358480287881
H	5.35928869884159	31.15244510419229	19.04332174069608
C	5.10362369450934	27.96884929045826	13.57873486220450
H	4.48475619826235	28.54454834177291	12.86643283216809
H	4.80241778085780	26.91315429160306	13.50592437394724
H	6.14690570887833	28.04112107713364	13.24325055439005
C	5.37296971201795	30.03863157104664	14.94243642956246
H	4.89141682735863	30.57437519408461	14.10353343782842
H	6.46590838255760	30.07860367506211	14.78994805087569
H	5.14354248496805	30.57834323602059	15.87654716190528
C	3.33847208709145	28.55247609262632	15.21311244407288
H	2.83563198236111	28.97923576683193	14.32685176147011
H	3.01831042931997	29.14536053816269	16.08531405230702
H	2.96699486046171	27.52199748875039	15.35086025788610
C	7.69713552209739	27.81785307970974	20.13575054669482
C	8.47448013164333	29.01702410012469	20.15112751954936
C	9.36843208804165	29.21977175186198	21.21647394755788
H	9.96998789345154	30.13529619145467	21.24647350595522
C	9.49574974517700	28.28001758046542	22.25161084966268
H	10.1932683924476	28.46233422747464	23.07864475123201
C	8.72230433175950	27.11395720720569	22.22348079911131
H	8.81265135236811	26.38166996503741	23.03430676717636

$L^{tBu}CoOCoL^{tBu}$

Co	-3.13377753809389	3.07378229033125	17.37966214852013
Co	-5.45924574779238	4.23624686024651	19.58857466310224
O	-4.18413216818778	3.83921027757140	18.50491384320510
N	-6.34690670507176	3.31758851032229	20.98777503472765
N	-6.40361939722532	5.89250984026087	19.55188773468333
C	-8.67817357511030	2.57127624485501	21.77392277120834
C	-7.66470566527026	3.60422648688880	21.16866051691908
C	-8.21850082707133	4.80483388166122	20.68283901894907
H	-9.27729779331618	4.92345358953812	20.89671863508452
C	-7.63139607679846	5.95883327588207	20.08161541448252
C	-8.13994607214257	1.66637308678147	22.90808653492655
H	-8.97113170351857	1.02853796298722	23.26055194993374
H	-7.77340038397527	2.24883173147741	23.76833919732611
H	-7.32694885310256	1.00337030043680	22.58474846841851
C	-9.09928411031228	1.67130442066948	20.58322284661856
H	-9.82683152909637	0.90820436342624	20.91737014921023
H	-8.22764068439481	1.14997131382487	20.15611396015153
H	-9.56411503503027	2.27103745548794	19.78100236461809
C	-9.95193631129882	3.25318191109959	22.33412574560982
H	-10.5853991069010	2.48685695635420	22.81491958362260
H	-10.5680490530631	3.72889959215718	21.55233375883298
H	-9.70857730437158	4.01435153162156	23.09707029471877
C	-8.53285904355505	7.23411739114658	20.16417215332896
C	-8.84163877735539	7.48384278939212	21.66587148306774
H	-7.90615290038491	7.65598617551916	22.22832125317904
H	-9.36421560170676	6.63565657224749	22.13729721896004
H	-9.47628829811215	8.38287311643052	21.77267671312661
C	-9.84935214461311	6.96037006491053	19.39135590852787
H	-10.4958456454772	7.85618923284700	19.42999964043020
H	-10.4230504376642	6.11617102172920	19.80921619167432
H	-9.64049851617865	6.73556912235462	18.33081453691703
C	-7.94891269320021	8.55370799962815	19.61610617789700
H	-7.01962201211103	8.84810177677433	20.12743946645366
H	-8.69636812183318	9.34914000621658	19.79221545453676
H	-7.74114149772433	8.52145078382554	18.53653203127680
C	-5.57320477251995	2.51859038487340	21.88148516813296
C	-5.18401118506798	3.10121518114822	23.12594423426817
C	-4.51620948343821	2.29519603426906	24.06523386173362
H	-4.23589962439878	2.72192749192894	25.03568764064683
C	-4.18542994253161	0.96280021125886	23.77821362455983
H	-3.67478328962965	0.34534752379285	24.52741093002922
C	-4.46665156675809	0.44592793322876	22.50701191214421
H	-4.15571254711102	-0.57695962050492	22.25880109796970
C	-5.14162259884707	1.20935897788284	21.53495370700798
C	-5.43738287212315	4.57839123091487	23.41507778873095

C	7.81935027848898	26.85677320466372	21.17500866728144
C	8.33314244783555	30.05532239653097	19.04086066341879
H	7.26859638796409	30.08183867412973	18.74519693273754
C	8.70934113547510	31.48241802684345	19.46539871476518
H	8.46293214578350	32.19282069591650	18.65587776485578
H	9.79165412309242	31.58232683966904	19.66833159203374
H	8.16298343129658	31.79629078389917	20.37337784297235
C	9.11618794606461	29.62046571071085	17.79109933048700
H	8.81513226255705	28.60755167428628	17.47909367427708
H	10.2016188856433	29.60458729014735	17.99579468473233
H	8.93053535022665	30.31107184897039	16.94817565609616
C	6.95702448358682	25.60329192934051	21.22783086125597
H	6.38741605468324	25.54601242208778	20.28530410864616
C	5.93411723453686	25.66015346976632	22.38103394971981
H	5.25771775353561	26.52813940285606	22.29227025002732
H	6.44196981984812	25.72847807451174	23.36137567353663
H	5.31205435975718	24.74638278173792	22.38530712871357
C	7.81417330993976	24.33048271360625	21.33433297109642
H	8.63794045325565	24.32502566026299	20.60125480292124
H	7.19833750030841	23.43124214859296	21.16434067861612
H	8.28041652882943	24.24186890522660	22.33078493685506
C	6.91568141214656	26.23534213018939	14.95097649041801
C	6.26673313060117	25.02288453533102	14.58911037328125
C	6.61549069985030	24.42219736232154	13.36472245199333
H	6.10610584408714	23.49982647278946	13.06278685166610
C	7.58763367729051	24.98499070573030	12.52805995767318
H	7.82402470921494	24.51648970720871	11.56483307790440
C	8.27611394799098	26.13552956932843	12.93988743518923
H	9.06822387079347	26.54929991629300	12.30403213816550
C	7.96686773081038	26.77045593714027	14.15573553572195
C	5.18608266338552	24.39008622336481	15.45774041725353
H	5.18776077935502	24.91483809138959	16.42889574450689
C	3.78331448248837	24.55434086361420	14.84059845710428
H	3.51844859482283	25.61618849559573	14.70261325707224
H	3.01780215948342	24.09597514182266	15.49311529180715
H	3.72538581838255	24.06205462378556	13.85164125425279
C	5.48688331242873	22.90612976436779	15.73013225870546
H	6.52681218857544	22.74609050312387	16.05806928605168
H	5.33783412447531	22.29311554159280	14.82427149071034
H	4.81939760697604	22.51510790311879	16.51782608913135
C	8.75212213725577	27.99123810959068	14.61276622610262
H	8.16524834886725	28.47579326826424	15.41241688300476
C	10.0904108049376	27.53941887638371	15.23038166421933
H	9.92651262746945	26.80765901057428	16.04000629135776
H	10.6457570082370	28.40023007060021	15.64379722328598
H	10.7250067720190	27.05607500721567	14.46568920989237
C	8.97846210850299	29.03266184253006	13.50352100493142
H	8.02806027589556	29.34304788792945	13.03369104332761
H	9.63791445953592	28.64576447698517	12.70501458911221
H	9.46313701238922	29.93405827722589	13.92065280039687
H	-5.48746959495396	5.07661288566134	22.42779556456626
C	-4.28517884291169	5.22010926675743	24.20872093420082
H	-4.39929988089835	6.31888400081564	24.22123092448779
H	-3.30426074885567	4.98013048339727	23.76370262266293
H	-4.27318343091934	4.88191789798778	25.26143128123851
C	-6.77610668254082	4.84364021108671	24.13126682440911
H	-7.63321360403685	4.52480608402490	23.51864871854727
H	-6.89711438947328	5.92390517331208	24.33313341487610
H	-6.81790235326008	4.30800982683591	25.09832488971422
C	-5.37651772035050	0.60515467447966	20.15803343815897
H	-5.96623395721180	1.33518406378478	19.57478103259000
C	-4.03460679474421	0.39513056796267	19.42984863369396
H	-3.52755990575240	1.35779016033502	19.23741952984501
H	-4.19075465761482	-0.09712048494780	18.45520306633344
H	-3.35407899728309	-0.24335616237684	20.02264691760847
C	-6.16380362743907	-0.71805668173546	20.22970628841541
H	-7.11149622006610	-0.60535031373589	20.78418516838367
H	-5.57498161047033	-1.50654621458579	20.73338804713643
H	-6.40201773355500	-1.08243073978290	19.21409242597067
C	-5.71889104085603	6.94483530062091	18.86688821742642
C	-5.92747311390356	7.12519687609508	17.47398031349889
C	-5.27568705426615	8.19727466977124	16.83532504410346
H	-5.44212985367990	8.35935044543201	15.76288891986572
C	-4.41630709340024	9.05077425434343	17.53875284354761
H	-3.92475951338245	9.88594308811551	17.02463482875087
C	-4.15693016207967	8.80538574970853	18.89526038933134
H	-3.44944808554755	9.44573356036896	19.43575199530516
C	-4.79111795722216	7.75252384897659	19.57791179829199
C	-6.79170684660028	6.17689296767842	16.65449793445271
H	-7.26602959061856	5.46328786153082	17.35269443263545
C	-5.89795804706013	5.37116849027988	15.69418068691960
H	-5.12156544988433	4.81576373560752	16.24793206452017
H	-5.38509724665892	6.04046860498498	14.97951682606158
H	-6.48745615935979	4.64279366939216	15.11335781827874
C	-7.91306965459134	6.90250221026513	15.88763074458255
H	-7.50107098901582	7.59074597185442	15.12656979502312
H	-8.55372555108671	7.49709608465768	16.56293986303853
H	-8.55392144720258	6.17188162827497	15.36118809747673
C	-4.44006428427745	7.44174958697830	21.02453701890841
H	-5.26924029205445	6.84243640190120	21.44457601172105
C	-3.17131129041669	6.56673052762708	21.03053779711491
H	-3.33883486622336	5.62698300044702	20.47344221437472
H	-2.86017052236149	6.30813970430126	22.05692152828397
H	-2.33436606243427	7.08884945150916	20.53575951610765
C	-4.27895161457244	8.68984006350091	21.90679156451470
H	-5.17669659622464	9.33345444892334	21.86792101140156
H	-3.40989136621815	9.30158066291087	21.60253439308189
H	-4.11549638039988	8.39374936090216	22.95877875858672
N	-1.23405792675512	3.16338550441589	17.51109297131588
N	-3.35829741397303	1.96663749222432	15.86247668889557

N	10.4335659648025	21.30787724297569	16.56598280498759
N	11.5623124071407	22.65085210029934	18.89702726721091
C	12.1077569933478	19.63056115528211	15.49158036796572
C	11.6584463850173	20.76249296734719	16.48604846178227
C	12.6735356990644	21.14007972847553	17.39734911307154
H	13.6271595992948	20.64748850174080	17.21872162993402
C	12.6595765774809	21.94778884831942	18.55685585646970
C	14.01378826425431	21.91084027929540	19.35254867395973
C	11.07722454754147	19.13714759336409	14.45229408905308
H	11.53490743834149	18.29475863937584	13.90179324790961
H	10.80912113351713	19.90791367969914	13.71489839895331
H	10.14477954874661	18.77111784963988	14.90610070462866
C	13.34707786240672	20.11313236408850	14.69191558044857
H	13.67742749154000	19.31036944839835	14.00777430127933
H	14.20098620669393	20.37328901038444	15.33911221379823
H	13.10556078769856	20.99951742849574	14.07888758237657
C	12.50832291699759	18.39657031048826	16.34698300711485
H	12.81326378555521	17.56683309576895	15.68326603400294
H	11.65911963196698	18.04877507881016	16.96049553993850
H	13.34638654374173	18.61091287643348	17.03011817371735
C	15.12173240277976	22.45174909978637	18.40758069959684
H	16.09658381498093	22.43141700977983	18.92833113113500
H	14.91307565150347	23.49598306964293	18.11482089624651
H	15.21971914712421	21.85864843972383	17.48330017703257
C	14.11072335588597	22.72755660001237	20.65996004330512
H	15.14916310130273	22.64184690426346	21.02949478290566
H	13.44378494217826	22.35312522932528	21.45005484207259
H	13.89435340050091	23.79568980384829	20.52084204366540
C	14.32873107883546	20.43910995946370	19.73126780047270
H	15.26677908416003	20.39907664279605	20.31477301841853
H	14.45334115105305	19.78757599253159	18.85078295055227
H	13.52267271075340	20.01319095252084	20.35336337352004
C	9.36420323663318	21.09433892454600	15.64944283998992
C	8.27459941972950	20.25791174841426	16.01693977357808
C	7.26437095234863	20.03631028393933	15.06180113876445
H	6.42836594448901	19.37165499839606	15.31208799482610
C	7.30503007147357	20.65105839595110	13.80362098690038
H	6.51058050523048	20.45928686201384	13.07161530456565
C	8.35055724874366	21.53292918605703	13.48870181266183
H	8.36426068227528	22.02360717531872	12.51040724827154
C	9.39331213743764	21.77668963712902	14.39784931420813
C	8.21728838887680	19.56118713258133	17.37249325485350
H	8.95796251391552	20.05891367461623	18.02465092378643
C	6.83744441228449	19.70292101939463	18.03968263202338
H	6.55184337997864	20.76387376075094	18.11594942485301
H	6.86531475629813	19.28002547098404	19.06041531680621
H	6.05585762741749	19.15884662108500	17.47739327495967
C	8.61304371028460	18.07505679508328	17.26092992708166
H	9.62644461805317	17.95065397140116	16.84444581665030
H	7.91131414543947	17.52771780168404	16.60381544722069
C	-2.69250383022620	-0.31421457759279	14.89163956491143
C	-2.39112894026669	1.03753353396002	15.62587078309344
C	-1.10011952901475	1.18048539170975	16.16850733432871
H	-0.41164362487681	0.38601100318383	15.89360457033514
C	-0.48251845943236	2.23404924817751	16.90898697156933
C	1.07977284744354	2.19759170842833	16.86892958582198
C	-3.28230675313664	-1.24432384760439	15.98390279408232
H	-3.51783381952634	-2.23675143834741	15.55629160901576
H	-4.21051443222679	-0.82132414967739	16.40047714002428
H	-2.56734271432159	-1.38102720334402	16.81421591320236
C	-3.69563836780937	-0.24736902845268	13.71485399657455
H	-3.36215091004607	0.43739084198160	12.91892503324680
H	-4.70231799737643	0.06521968867518	14.02234590053869
H	-3.77893762101220	-1.25941930115618	13.27807247989326
C	-1.41117247555437	-0.98217555835960	14.33358936865114
H	-0.86481686460844	-0.31276351666136	13.64497433161003
H	-1.69663987689528	-1.88585860950770	13.76652050939149
H	-0.71549189369242	-1.31006992760701	15.12466486502756
C	1.49520468663032	2.30508894777476	15.37623142787738
H	1.08506201319312	1.48387367149309	14.76581284159687
H	2.59737709235021	2.28436729334883	15.29013793069032
H	1.13531009934256	3.25636615225282	14.94400634145584
C	1.56718402029816	0.84858470977684	17.45964625135410
H	1.22938920319268	0.73448241956870	18.50472109909392
H	2.67207865581364	0.81957378249721	17.45270305955048
H	1.20883602840644	-0.02547292141921	16.89079276066968
C	1.83663843526221	3.31485712832474	17.61799721902207
H	1.65588852354529	3.30649217018102	18.70300251694960
H	1.58729082502284	4.31982407795045	17.24565511925551
H	2.91833094305136	3.15450157735045	17.45477846973992
C	-4.39640172228455	2.28249882455433	14.93723397127185
C	-4.03968554238276	3.02012833844505	13.76802012609627
C	-5.02581793498367	3.25122623551321	12.79237520475465
H	-4.75851751377980	3.79233354687121	11.87648187735451
C	-6.34741935928019	2.81880084023840	12.97600797574082
H	-7.10132213706317	2.99697791358241	12.19937105844951
C	-6.70577380818360	2.20275467968028	14.18249396726038
H	-7.75143060949502	1.91577126173763	14.35268150512192
C	-5.75333835654647	1.94067029411574	15.18610500104839
C	-2.63483669090446	3.59268763559343	13.59844483627409
H	-2.20571170614926	3.66034144182182	14.61618109423502
C	-2.66334738544475	5.01402168616909	13.00831405254918
H	-1.66098331978617	5.47368906545733	13.07434291165505
H	-3.37509270555393	5.65875485086409	13.55161221085119
H	-2.95203749186485	5.01090570716322	11.94105858974017
C	-1.70178804122881	2.69211475056575	12.76638274074387
H	-2.11439020260610	2.52484882501560	11.75361026587358
H	-1.55312965990436	1.71242759228358	13.24622008746585
H	-0.70747742246906	3.16298078035478	12.65791220958459
C	-6.21131543407471	1.30839057649145	16.49232729998469

H	8.59417544860859	17.59225361931011	18.25541427289296
C	10.56279429892097	22.69589155865462	14.05651930368936
H	11.47878378771620	22.20173607748261	14.42972945137906
C	10.45491953681399	24.04228133295679	14.79438136722198
H	10.48122119168918	23.91379338341399	15.89318489670643
H	9.51055115048130	24.55464148900304	14.55370397397726
H	11.29482262625532	24.70553269410523	14.52139934007844
C	10.75805099395491	22.91739357091087	12.54928140542847
H	10.82960765741099	21.96092058443335	12.00006025597737
H	11.68914453194513	23.48439410131644	12.37053282546247
H	9.92904317975868	23.50314586154816	12.11509237495664
C	11.36256527838074	23.28758625541096	20.15620740420825
C	11.50318348251458	24.69834514676661	20.25482409862782
C	11.38374960933366	25.28774707485305	21.52627457497033
H	11.51485161261246	26.37081555582690	21.62751910528804
C	11.09213745680638	24.51679876554835	22.65956673332593
H	11.01354426990360	24.99446610494986	23.64406131325707
C	10.86203346592256	23.13930496787288	22.52637218232016
H	10.58993028246512	22.54883874934733	23.40989661224917
C	10.98345986657829	22.49880369286501	21.28057804143193
C	11.82022199797994	25.55958068712108	19.03774952116796
H	11.67682244624901	24.92580993645467	18.14223715581927
C	10.85517176526689	26.74877913692743	18.93012720210307
H	9.80950744817566	26.40612968541098	18.88111093213745
H	11.06702143123120	27.32909687287755	18.01647833508195
H	10.94376240338186	27.43450161930009	19.79059645159733
C	13.28080671587268	26.05323807706038	19.03559090866313
H	14.00025852906713	25.21750820898186	19.02413860136532
H	13.49065117766052	26.66701675159558	19.93160148996356
H	13.47463754825979	26.67765254728672	18.14415085012659
C	10.69999768371516	21.00623747898424	21.14318672198624
H	11.13628893543413	20.66929360219353	20.18541501072445
C	11.33644937362258	20.16595622153847	22.26505077179236
H	12.41897895964505	20.36399274017827	22.36250104386745
H	11.20245627696320	19.08850745282490	22.05915252996247
H	10.86853159217330	20.37230639555635	23.24516497036085
C	9.17831980038271	20.75939643327582	21.06326600881891
H	8.71756803492985	21.33582230826914	20.24381425563770
H	8.68748139753894	21.06330747097008	22.00675916010428
H	8.96651531421888	19.68679744439182	20.89736156709949
H	-5.30993532149189	1.14329362919719	17.10969819278245
C	-7.13722798248775	2.27116152281904	17.26087176105831
H	-6.59811989928135	3.18614962230982	17.56598676011670
H	-7.52378527705249	1.79517633940212	18.17787503366599
H	-8.00589887104337	2.56874334414670	16.64524263693800
C	-6.90725925160550	-0.04815911835851	16.26734530435836
H	-6.27667427589237	-0.74379341013803	15.68681724787746
H	-7.85848511765458	0.07677146237574	15.71797070641166
H	-7.14467058911513	-0.52645192589281	17.23467565564552
C	-0.76418509137279	4.23121384739746	18.33820022762301
C	-0.55774985455594	4.00131472231357	19.72448899210690
C	-0.05941933014002	5.05812960640213	20.50908283833911
H	0.11969645694736	4.88979825645709	21.57859477740587
C	0.19849044909104	6.31894620563768	19.95470722404410
H	0.59338141707663	7.12788448305770	20.58172229523653
C	-0.09315862895617	6.55072003668564	18.60274547318977
H	0.06240783439120	7.55022944164844	18.17789892069773
C	-0.58429598346847	5.52308356323889	17.77752816161487
C	-0.90591004841303	2.67443511192133	20.38463840155710
H	-1.22325391536003	1.97514984134829	19.58977041597430
C	-2.09982674816550	2.87644391304618	21.33500344775019
H	-2.96900758169191	3.28683545062478	20.79384380234558
H	-1.84488124946252	3.58460223882394	22.14439599020665
H	-2.40761815759438	1.92587135195547	21.80090266808357
C	0.28845632184490	2.04043490731812	21.12179936145933
H	1.15396634690660	1.89328946515998	20.45149895146899
H	0.00551420787110	1.05578023472013	21.53662869249078
H	0.62315391380925	2.67206305121626	21.96545577625398
C	-0.97035932895089	5.81566455010066	16.33618144739172
H	-1.12798944700659	4.84533846700180	15.83173677987173
C	-2.31266589049147	6.57064211099749	16.33755846249015
H	-3.09669255598194	5.98513232415480	16.84914360854848
H	-2.65674154508873	6.78593036020383	15.31115925138454
H	-2.22288065218473	7.52895768925434	16.87788010721153
C	0.11637485017316	6.57480974670198	15.55642102613021
H	0.29517473346916	7.58193500928809	15.97592761724832
H	-0.18927579705350	6.70828856748602	14.50281309606158
H	1.07782907858994	6.02977865798034	15.56666447260357

O. Comparison of diketiminate bond metrics between 3 and $L^{tBu}CoCl$

For additional evidence that oxo complex **3** contains cobalt(II) ions, we compared the diketiminate bond metrics of the oxo (right ORTEP diagram) to the known three-coordinate cobalt(II) complex $L^{tBu}CoCl$ (left ORTEP diagram; from ref. 1 of ESI). All ligand backbone bonds are within error between the two compounds, arguing against ligand redox activity within the diketiminate supporting ligand.

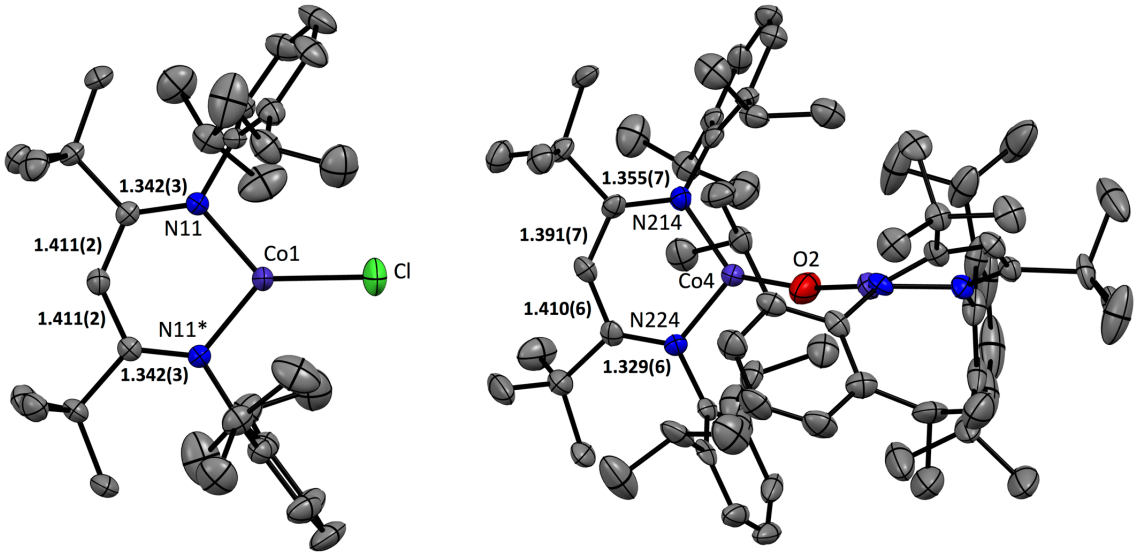

P. Electronic structure of 3 from multi-configurational calculations.

Table S5. Configuration state functions with weight % for the first root calculation of complex **3**, obtained by **CASSCF(20,13)**. (2: doubly occupied MO, 0: unoccupied MO, 1: singly occupied MO with charge = 0, multiplicity = 1, E= -5297.8932652040 hartree)

CSF	Weight %
2221111121222	0.29
2221111212122	0.34
2221111221122	0.45
2221112212112	0.90
2221112221112	1.22
2221112222111	0.45
2221121121221	0.94
2221121221121	1.48
2221121221211	0.55
2221122121211	0.41
2221122212111	0.45
2221122221111	3.95
2221211112122	0.51
2221211112212	1.06
2221211121122	0.68
2221211121212	1.45
2221211122211	0.54
2221212112112	0.94
2221212121112	1.30
2221212122111	0.47
2221221112121	0.26
2221221112211	0.53
2221221121121	2.23

CSF	Weight %
2221221121211	4.65
2221221221111	0.50
2221222112111	0.47
2221222121111	4.15
2222111111222	0.45
2222111112221	1.24
2222111211122	0.70
2222111211212	0.26
2222111212121	1.98
2222111212211	0.75
2222111221121	0.32
2222112112211	0.55
2222112211112	1.89
2222112212111	5.24
2222112221111	0.84
2222121111221	1.15
2222121211121	1.85
2222121211211	0.68
2222122111211	0.51
2222122211111	4.87
2222211111122	1.08
2222211111212	2.23
2222211112121	2.97

CSF	Weight %
2222211112211	6.20
2222211121121	0.49
2222211121211	0.98
2222211212111	0.65
2222212111112	2.01
2222212112111	5.51
2222212121111	0.88
2222221111121	2.78
2222221111211	5.74
2222221211111	0.61
2222222111111	5.09

Table S5 shows that the first root of the CAS(20,13) calculation on intermediate 3 has several competing electronic configurations and has significant multiconfigurational character. However, all the CSFs reveal that the oxygen-based ligand orbitals, which are lowest in energy, are never singly occupied; they have predominantly oxygen n_π orbital character. This analysis confirms that the oxygen center has all p-orbitals filled and is best described as O^{2-}, i.e, intermediate **3** has relatively polar bonds and is best described as Co^{2+}-O^{2-}-Co^{2+}.

Figure S18. Natural orbitals for CASSCF(24,17) calculation at S=0 with def2-TZVPP basis set. Atomic contributions and occupancy (in parenthesis) are also shown.

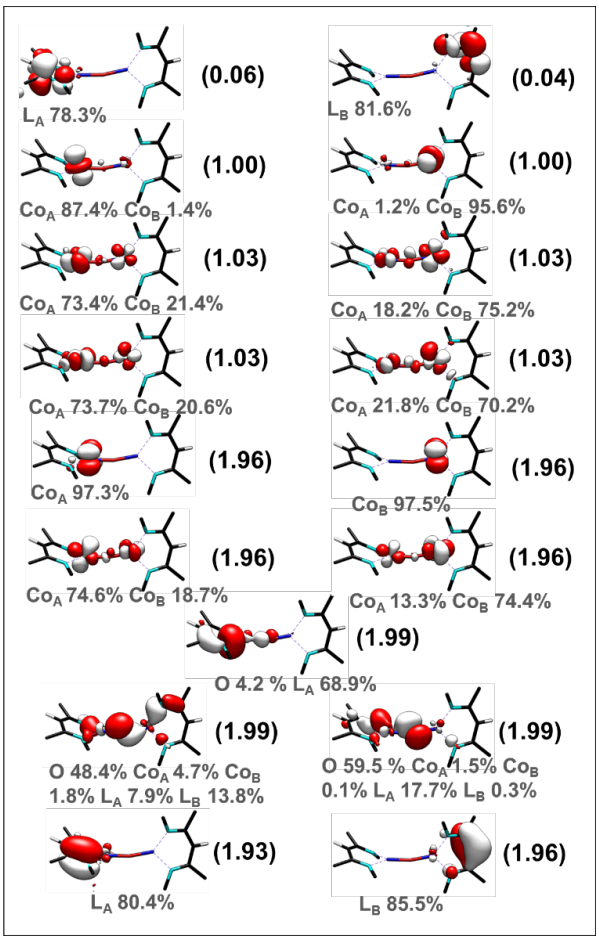

We constructed a larger active space considering the doubly-filled π and vacant π* orbitals of the β-diketiminate ligand in order to allow relaxation of the wave-function and explore excitation between these orbitals. The active space now consists of all metal based d-orbitals, the O centered p orbitals, and two high-lying π orbitals: one on each of the β-diketiminate ligands and their corresponding anti-bonding π* orbitals. This yielded an active space consisting of 24 electrons in 17 orbitals. In Figure S18, we have compared how the active space changes before and after calculation of CASSCF(24,17). Importantly, the π* orbitals of the β-diketiminate ligand were essentially vacant with occupation numbers in the range 0.04-0.06. Moreover, the π-orbitals of β-diketiminate ligand are not correlated to the Co-O-Co core (Figure S18) and the bonding between Co and the ligand N-C-N is primarily ionic in nature as evident from strong localization on the N-C-N motif (80-85%). Thus, inclusion of bonding and antibonding π orbitals of the β-diketiminate ligand does not change the overall description of the electronic structure of the cobalt centers as high-spin Co(II)**. This justifies the suitability of CASSCF(20,13) calculation for complex 3**.

Q. Frontier orbital analysis during dinuclear associative pathway

Figure S19. Important orbitals during C-O cleavage mediated by dinuclear associative pathway.

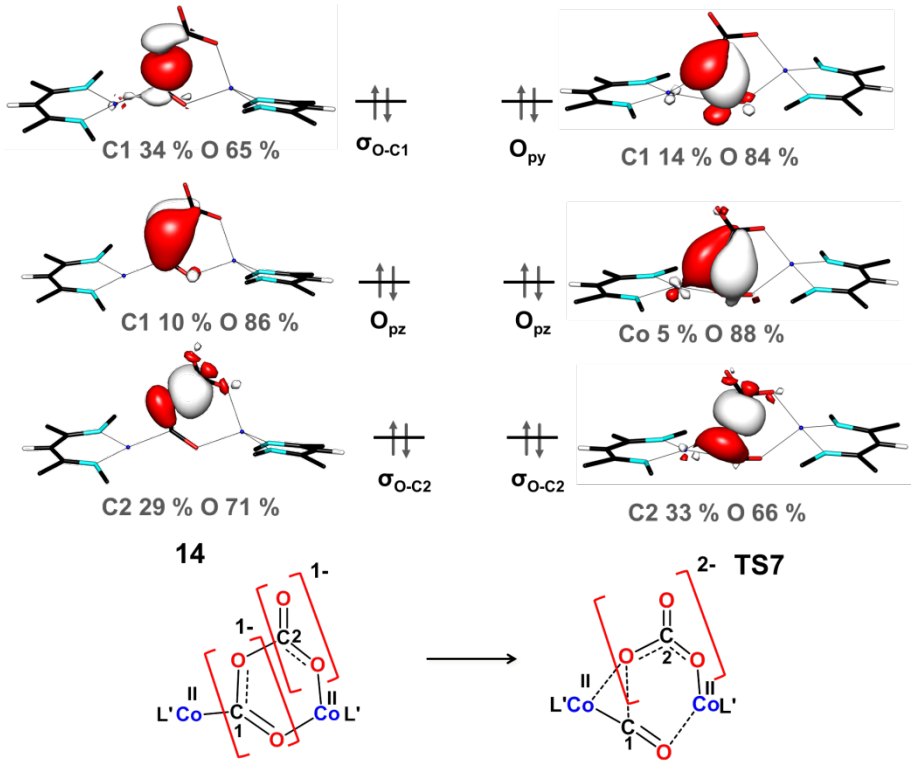

The dinuclear associative pathway involves heterolytic C-O bond cleavage via **TS7**. Here charge neutralization around the target oxygen center occurs due to interaction with the nearest metal center. The Lewis acidity of the metal center therefore plays a key role in facilitating the C-O bond scission. The Co-O interaction polarizes the target C-O bond, which may be responsible for the lower barrier pathway in the bimetallic species.

R. Thermodynamics of additional pathways with mononuclear species

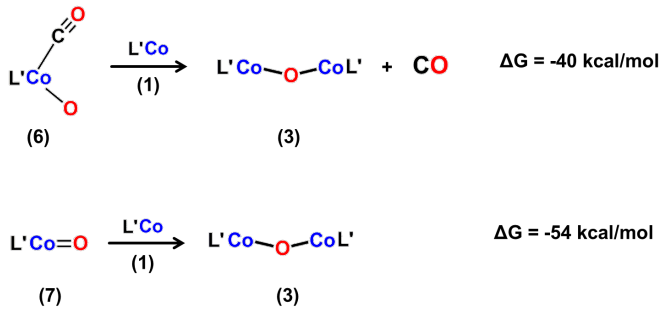

The formation of **3** from **6** or **7** in the presence of **1**, involving release of a CO molecule in **6** in the former reaction, was computed to have favorable driving forces; however, in the mononuclear dissociative pathway the generation of **6** and **7** has to transvers a high barrier for the C-O bond cleavage. Hence, these two pathways were not considered in the free energy profile in the main text.

S. Why the mononuclear associative pathway is not predicted

CO_2 is a linear non-polar molecule featuring very short C-O bond lengths (1.16 Å). Due to the electronegativity difference between C and O, it has partially positive carbon and partially negative oxygen. Activation of CO_2 is manifested by bending of the O-C-O angle (~ 130 °) and a decrease in the C-O bond order. To be noted that CO_2 has a carbon-localized LUMO and the large HOMO-LUMO gap in linear molecule is not conducive for nucleophilic/electrophilic attack. Bending of the molecule lowers the energy of its LUMO, primarily of the in-plane orbital, and increases the carbon weight in its LUMO and oxygen content in its HOMO. These factors enhance the electron accepting ability of CO_2. Hence reduction of CO_2 requires a synchronous bi-functional activation.[36]

To the best of our knowledge, the mononuclear associative pathway has not been discussed in the literature in the context of a $(CO_2)_2$ dimer formation. Agarwal and others have proposed a mononuclear associative pathway consisting of association of **formic acid with CO_2**.[37] In that paper, the presence of a proton on HCOOH ensures strong hydrogen bonding with oxygen of incoming CO_2 which should have promoted overall electron transfer process in the bent CO_2. However, the dissociative pathway is a more common prediction and there are several examples of both mononuclear and dinuclear dissociative pathways studied theoretically by several groups with the β-diketiminate ligand based metal complexes of Fe, Co and Mn.[38-41] However, only a single study by Agarwal and others discusses the dinuclear associative pathway for insertion of CO_2 into a rhenium carboxylate dimer, $[Re(dmb)(CO)_3]_2$, where dmb = 4,4′-dimethyl-2,2′-bipyridine, to release CO and form a carbonate-bridged rhenium dimer.[42] Hence to say associative pathway is a unique mechanistic channel studied in the present report which has very few precedence both for mononuclear and dinuclear cases.

Figure S20. Various CO_2 activation pathways studied in this report: (a) CO_2 addition to the starting material, (b) CO_2 activation by cobalt-oxo species in the mononuclear dissociative pathway, (c) CO_2 activation by bridging CO_2 complex in intermediate **10** during dinuclear associative pathway, (d) CO_2 activation by the μ-oxo dicobalt complex **3** in the dinuclear dissociative pathway and (e) the computationally unobserved association of CO_2 to the η^2-(C,O) adduct in intermediate **5** to a hypothetical **5'**.

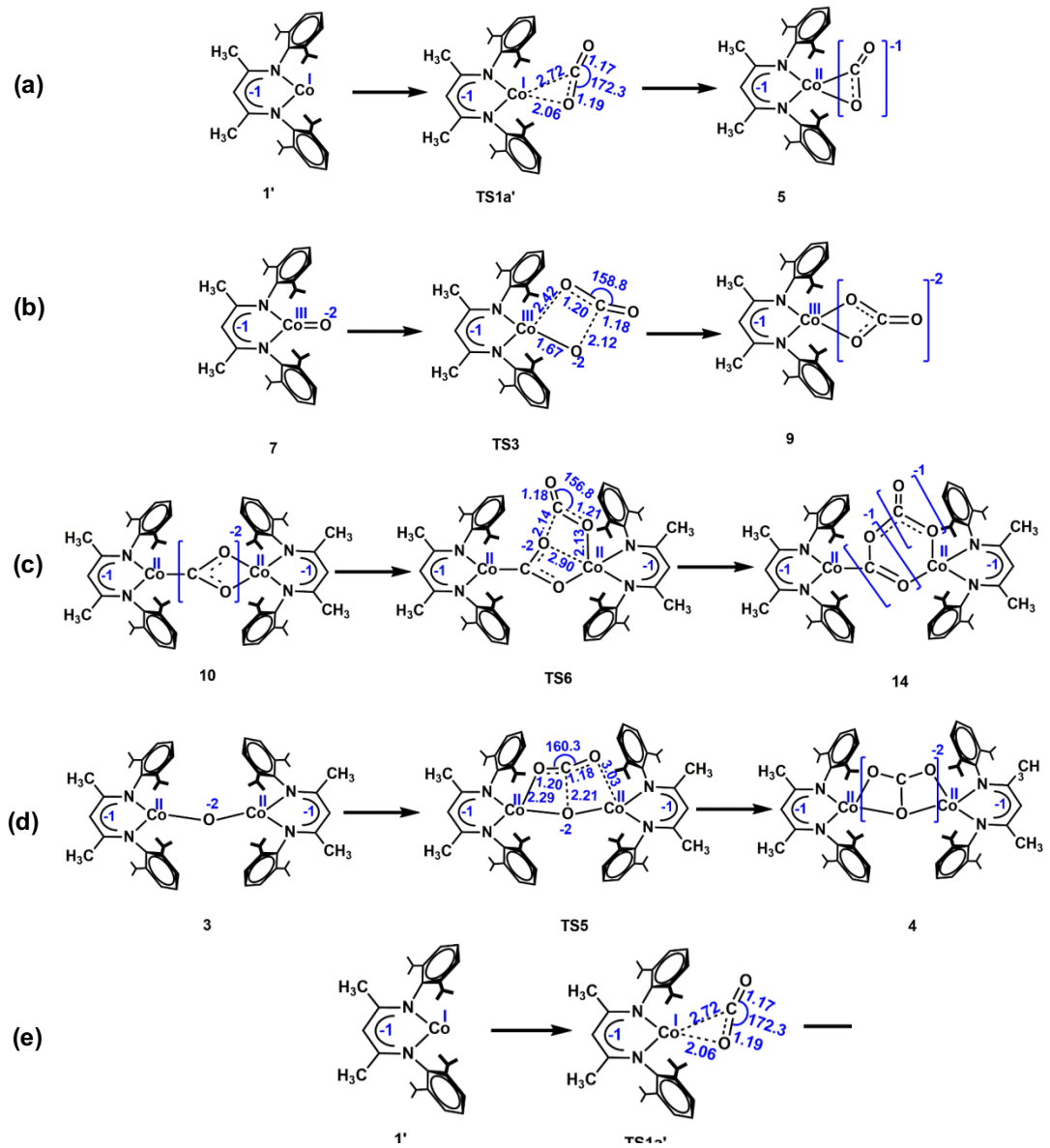

In the various CO_2 activation pathways that we have summarized above in Figure S20, we found that in each of the feasible pathways, CO_2 activation is manifested by cooperative effects of a Lewis acid (like a second metal center) and a Lewis base, electron-rich negatively charged oxo group or a two electron-reduced $[CO_2]^{2-}$. In intermediate **5**, there is only partial electron transfer from Co^{I} to bound CO_2 which makes it $[CO_2]^{-1}$ in charge. Therefore, the nucleophilicity or basicity of this bound CO_2 is not conducive to promote electron transfer to another incoming CO_2. Moreover, the lack of a neighbouring Lewis acid group which might help in bending of the incoming CO_2 prior to activation is also a reason that inhibits facile association of a second CO_2 unit to the mononuclear adduct **5** and hence a mononuclear associative pathway is not possible. However, during dinuclear associative pathway, the bridging CO_2 which is actually $[CO_2]^{2-}$ has conducive basicity for nucleophilic attack to

the carbon of an incoming CO_2. Secondly, the second CO_2 could properly anchor on one of the cobalt centres, which decreases the O-C-O angle to 156 °, and enhances the possibility of electron acceptance through the carbon-based CO_2 LUMO. These two factors are responsible for a plausible dinuclear associative pathway.

T. Total energies predicted at M06L(CPCM)/def-2TZVPP level of theory

Species	**Energy in a.u.**
1 (S = 1)	-2639.75459
TS1 (S = 1)	-2639.713401
1' (S = 1)	-2639.746122
CO_2 (S = 0)	-188.8549092
1a' (S = 1)	-2828.612371
TS1a' (S = 1)	-2828.609281
5 (S = 1)	-2828.618511
TS2 (S=1)	-2828.582323
6 (S = 1)	-2828.591359
2 (S = 1)	-2753.283541
7 (S = 1)	-2715.090548
8 (S = 1)	-2903.950627
TS3 (S = 1)	-2903.938293
9 (S = 1)	-2903.99207
TS2' (S = 2)	-5467.278893
10 (S = 3) **(S = 0)**	-5468.453273 -5468.454382
TS4 (S = 3) **(S = 0)**	-5468.417772 -5468.420127

11 (S = 3)	-5468.448698
(S = 0)	-5468.45327
3 (S = 3)	-5354.956605
(S = 0)	-5354.964939
12 (S = 3)	-5543.822192
(S = 0)	-5543.825493
TS5 (S = 3)	-5543.813262
(S = 0)	-5543.817719
4 (S = 3)	-5543.847435
(S = 0)	-5543.848663
13 (S = 3)	-5657.309157
(S = 0)	-5657.309298
TS6 (S = 3)	-5657.286463
(S = 0)	-5657.290172
14 (S = 3)	-5657.297302
(S = 0)	-5657.29552
TS7 (S = 3)	-5657.284506
(S = 0)	-5657.284082
15 (S = 3)	-5657.314354
(S =0)	-5657.314219

U. Electronic structure of Co-O-Co at different levels of Density Functional Theory.

Figure S21. Electronic structure of L′Co-O-CoL′ at (a) BP86 (S=3), (b) BP86 (S=0), (c) M06L (S=3), (d) M06L (S=0), (e) B3LYP (S=3) and (f) B3LYP (S=0) level of theory with the def2-TZVPP basis set.

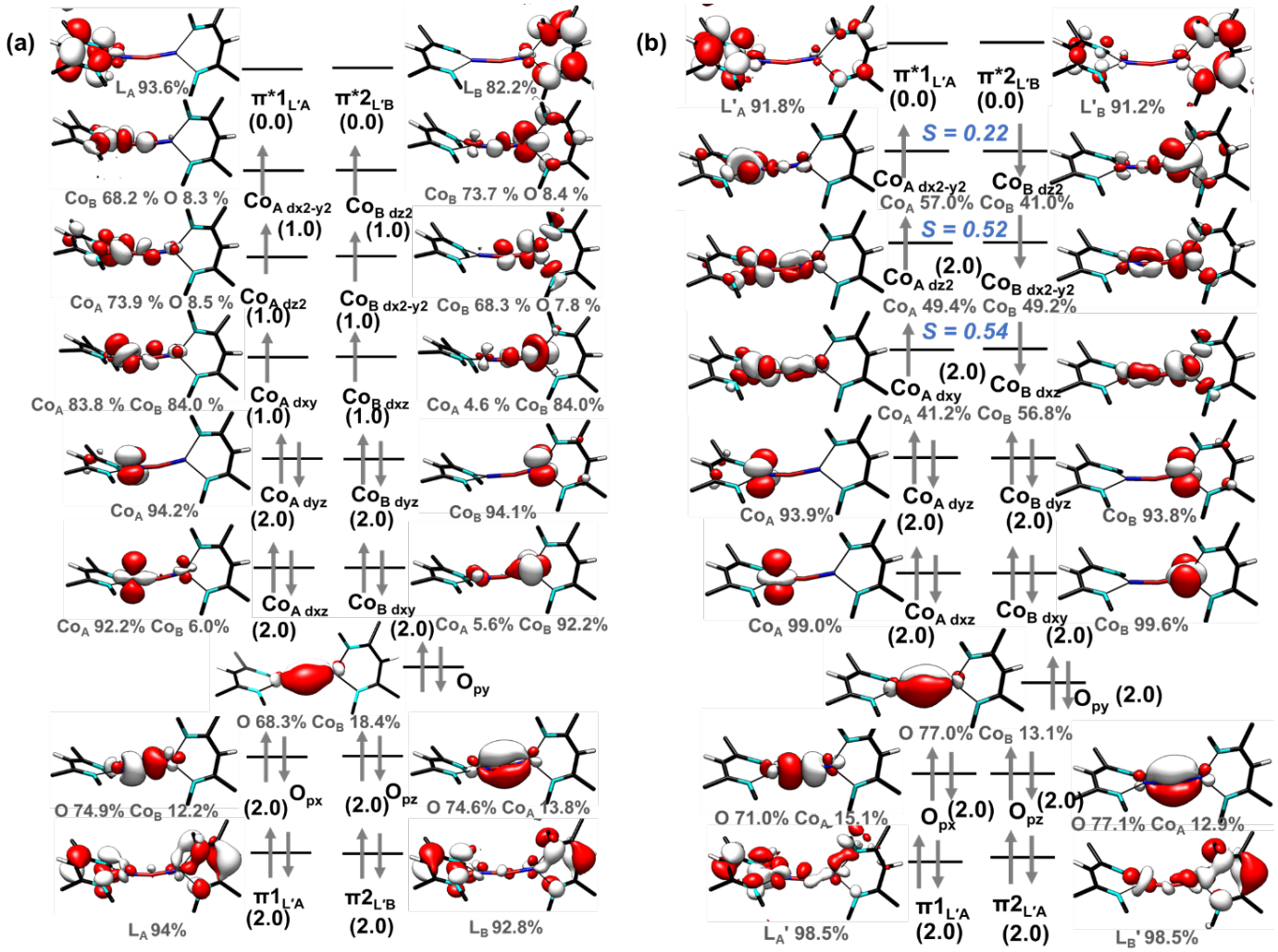

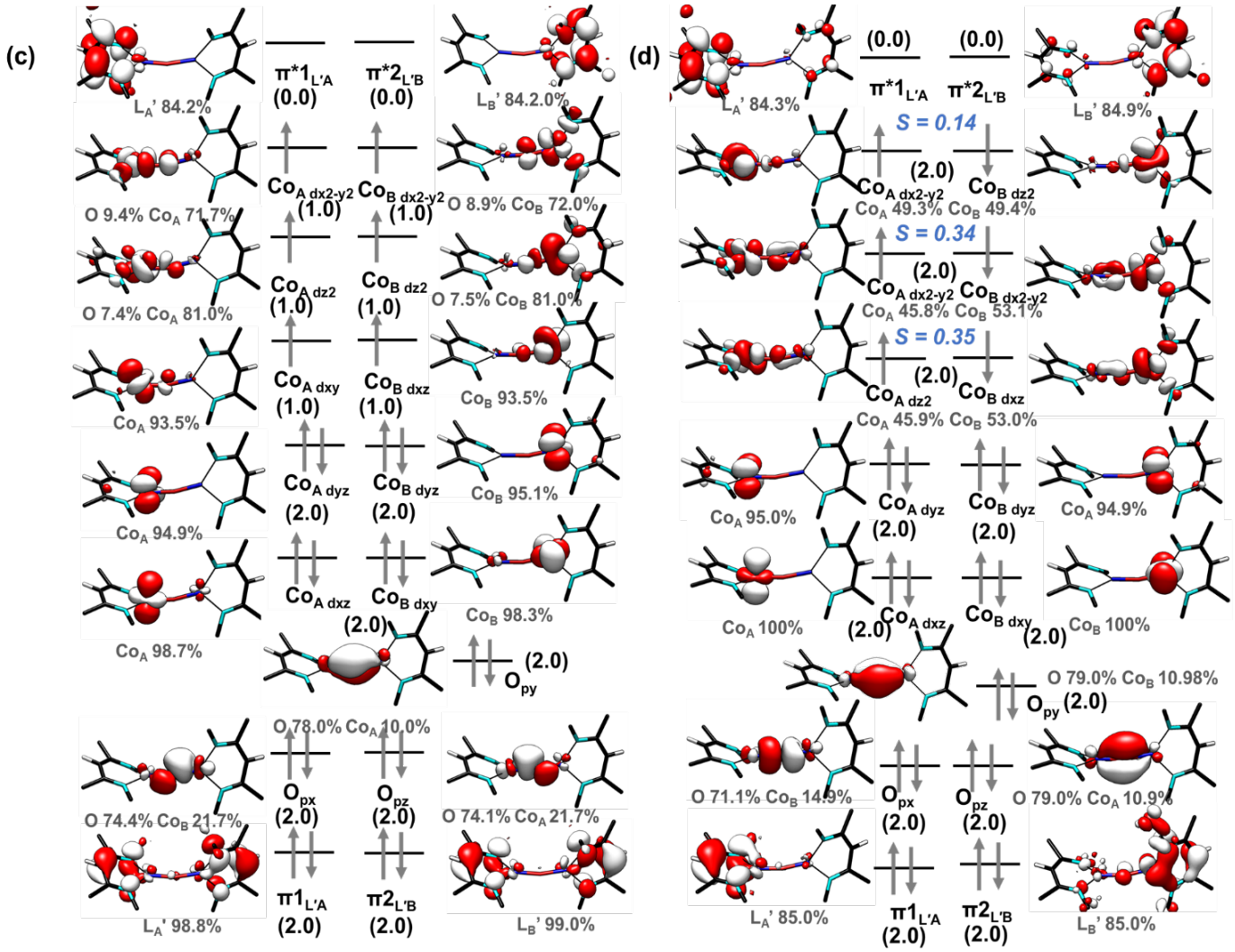
(c)
π*1L'A
(0.0)
π*2L'B
(0.0)
LA' 84.2%
LB' 84.2.0%
CoA dx2-y2
(1.0)
CoB dx2-y2
(1.0)
O 9.4% CoA 71.7%
O 8.9% CoB 72.0%
CoA dz2
(1.0)
CoB dz2
(1.0)
O 7.4% CoA 81.0%
O 7.5% CoB 81.0%
CoA dxy
(1.0)
CoB dxz
(1.0)
CoA 93.5%
CoB 93.5%
CoA dyz
(2.0)
CoB dyz
(2.0)
CoA 94.9%
CoB 95.1%
CoA dxz
(2.0)
CoB dxy
(2.0)
CoA 98.7%
CoB 98.3%
(2.0)
Opy
(2.0)
O 78.0% CoA 10.0%
Opx
(2.0)
Opz
(2.0)
O 74.4% CoB 21.7%
O 74.1% CoA 21.7%
π1L'A
(2.0)
π2L'B
(2.0)
LA' 98.8%
LB' 99.0%
(d)
π*1L'A
(0.0)
π*2L'B
(0.0)
LA' 84.3%
LB' 84.9%
S = 0.14
CoA dx2-y2
(2.0)
CoB dz2
CoA 49.3% CoB 49.4%
S = 0.34
CoA dx2-y2
(2.0)
CoB dx2-y2
CoA 45.8% CoB 53.1%
S = 0.35
CoA dz2
(2.0)
CoB dxz
CoA 45.9% CoB 53.0%
CoA 95.0%
CoA dyz
(2.0)
CoB dyz
(2.0)
CoA 94.9%
CoA 100%
CoA dxz
(2.0)
CoB dxy
(2.0)
CoB 100%
O 79.0% CoB 10.98%
Opy (2.0)
O 71.1% CoB 14.9%
Opx
(2.0)
Opz
(2.0)
O 79.0% CoA 10.9%
LA' 85.0%
π1L'A
(2.0)
π2L'B
(2.0)
LB' 85.0%

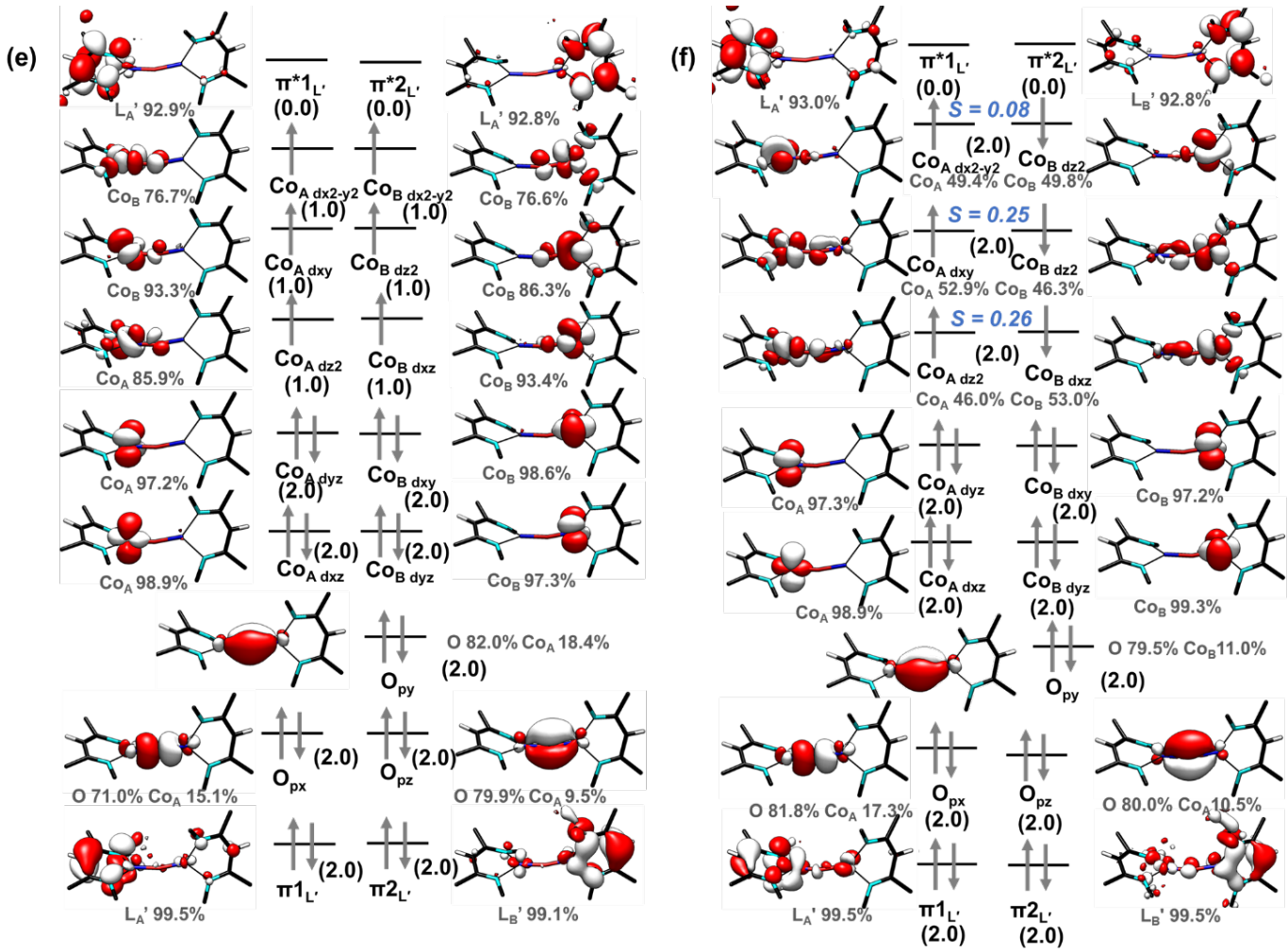

The choice of functional can have important influences on the result of a computational study, and therefore we used several different density functionals: BP86 (which is a local gradient corrected functional consisting of Becke's exchange and Perdew's correlation), M06L (the local meta-GGA functional developed by Truhlar and co-workers) and the most popular hybrid functional, B3LYP (consisting of 20% Hartree Fock exchange) to evaluate the electronic structure of intermediate **3**. High-spin models using **each of these functionals** gave quasi-restricted DFT orbitals consistent with a d^7 configuration at cobalt, with 4 electrons in the doubly-occupied region and 3 electrons in the singly occupied region. The doubly occupied orbitals have > 90% Co d-parentage while the singly occupied orbitals have ~ 70-90% contribution from metal-based d-orbitals. This is also true for the broken-symmetry models, where we also found three anti-ferromagnetic coupling (for e.g. small overlap in the range of 0.5 to 0.2 at BP86/def-TZVPP level) between the non-orthogonal orbitals of either metal site, in addition to four uncoupled doubly occupied orbitals. **Therefore, analysis of electron occupancy with different HF exchange indicate unanimously the dicobalt(II) oxo electronic structure**. The schematic representation of the electronic structure of species **3** (both with S=0 and S=3) along with occupancy and atomic contributions to each orbitals with these three different functionals containing different % HF exchange is provided above in Figure S21.

Figure S22. Molecular electrostatic potential (MEP) surface of intermediate **3** at BP86/def2-TZVPP. Value of isosurface = 0.02 au. The color spectrum ranges from negative (blue) to positive (red) electrostatic potential within ±1.0e-2 a.u.

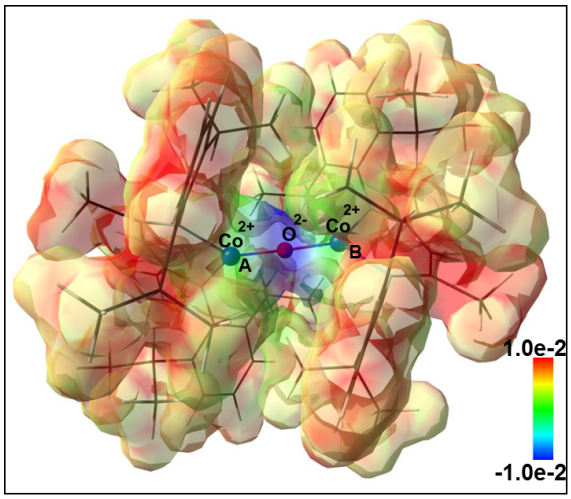

The MEP plot in Figure S22 reveals distribution of negative electrostatic potential (blue colored isosurface) centrally on oxygen and positive electrostatic potential (red colored isosurface) on some parts of the ligand. The cobalt centers are in the borderline region (green colored isosurface). The MEP mapping clearly shows that the oxygen in species **3** is enveloped by a negative electronic potential and explains the reason for its high reactivity.

Table S6. Mulliken gross atomic charges on intermediate **3** with different density functionals employing the def2-TZVPP basis set.

S = 3

Atom	**BP86**	**B3LYP**	**M06L**
Co_A	0.6380	0.7852	0.6762
O	-0.6812	-0.8504	-0.6881
Co_B	0.6411	0.7829	0.6857

S = 0

Atom	**BP86**	**B3LYP**	**M06L**
Co_A	0.6036	0.7706	0.6593
O	-0.6195	-0.8169	-0.6645
Co_B	0.5989	0.7689	0.6503

V. References for ESI

1. K. Ding, P. L. Holland, D. Adhikari and D. J. Mindiola, *Inorg. Synth.*, 2010, 35, 43-45.
2. T. R. Dugan, X. Sun, E. V. Rybak-Akimova, O. Olatunji-Ojo, T. R. Cundari and P. L. Holland, *J. Am. Chem. Soc.*, 2011, 133, 12418-12421.
3. M. H. Al-Afyouni, E. Suturina, S. Pathak, M. Atanasov, E. Bill, D. E. DeRosha, W. W. Brennessel, F. Neese and P. L. Holland, *J. Am. Chem. Soc.*, 2015, 137, 10689-10699.
4. A. D. Becke, *Phys. Rev. A*, 1988, 38, 3098-3100.
5. J. P. Perdew, *Phys. Rev. B*, 1986, 33, 8822-8824.
6. A. Schäfer, C. Huber and R. Ahlrichs, *J. Chem. Phys.*, 1994, 100, 5829-5835.
7. A. Schäfer, H. Horn and R. Ahlrichs, *J. Chem. Phys.*, 1992, 97, 2571-2577.
8. B. Kirchner, F. Wennmohs, S. Ye and F. Neese, *Curr. Opin. Chem. Biol.*, 2007, 11, 134-141.
9. L. Noodleman, *J. Chem. Phys.*, 1981, 74, 5737-5743.
10. F. Neese, *WIREs Comput. Mol. Sci.*, 2012, 2, 73-78.
11. F. Neese, *WIREs Comput. Mol. Sci.*, 2018, 8:e1327.
12. K. Eichkorn, Weigend, F., Treutler, O. et al., *Theor. Chem. Acta.*, 1997, 97, 119-124.
13. K. Eichkorn, O. Treutler, H. Öhm, M. Häser and R. Ahlrichs, *Chem. Phys. Lett.*, 1995, 242, 652-660.
14. K. Eichkorn, O. Treutler, H. Öhm, M. Häser and R. Ahlrichs, *Chem. Phys. Lett.*, 1995, 240, 283-290.
15. E. v. Lenthe, E. J. Baerends and J. G. Snijders, *J. Chem. Phys.*, 1993, 99, 4597-4610.
16. E. van Lenthe, E. J. Baerends and J. G. Snijders, *J. Chem. Phys.*, 1994, 101, 9783-9792.
17. E. van Lenthe, R. van Leeuwen, E. J. Baerends and J. G. Snijders, *Int. J. Quantum Chem.*, 1996, 57, 281-293.
18. D. A. Pantazis, X.-Y. Chen, C. R. Landis and F. Neese, *J. Chem. Theory Comput.*, 2008, 4, 908-919.
19. J. Tomasi, B. Mennucci and R. Cammi, *Chem. Rev.*, 2005, 105, 2999-3094.
20. C. Lee, W. Yang and R. G. Parr, *Phys. Rev. B*, 1988, 37, 785-789.
21. Y. Zhao and D. G. Truhlar, *J. Chem. Phys.*, 2006, 125, 194101.
22. F. Weigend and R. Ahlrichs, *Phys. Chem. Chem. Phys.*, 2005, 7, 3297-3305.
23. F. Neese, F. Wennmohs, A. Hansen and U. Becker, *Chem. Phys.*, 2009, 356, 98-109.
24. S. Grimme, S. Ehrlich and L. Goerigk, *J. Comput. Chem.*, 2011, 32, 1456-1465.
25. S. Grimme, J. Antony, S. Ehrlich and H. Krieg, *J. Chem. Phys.*, 2010, 132, 154104.
26. M. Saitow, U. Becker, C. Riplinger, E. F. Valeev and F. Neese, *J. Chem. Phys.*, 2017, 146, 164105.
27. C. Riplinger and F. Neese, *J. Chem. Phys.*, 2013, 138, 034106.
28. B. Mondal, F. Neese and S. Ye, *Inorg. Chem.*, 2015, 54, 7192-7198.
29. J. Song, E. L. Klein, F. Neese and S. Ye, *Inorg. Chem.*, 2014, 53, 7500-7507.
30. K. Ruedenberg, L. M. Cheung and S. T. Elbert, *Int. J. Quantum Chem.*, 1979, 16, 1069-1101.
31. B. O. Roos, P. R. Taylor and P. E. M. Siegbahn, *Chem. Phys.*, 1980, 48, 157-173.
32. C. Angeli, R. Cimiraglia, S. Evangelisti, T. Leininger and J. P. Malrieu, *J. Chem. Phys.*, 2001, 114, 10252-10264.
33. K. D. Finkelstein, C. J. Pollock, A. Lyndaker, T. Krawcyk and J. Conrad, *AIP Conf. Proc.*, 2016, 1741, 030009.
34. R. C. Walroth, J. T. Lukens, S. N. MacMillan, K. D. Finkelstein and K. M. Lancaster, *J. Am. Chem. Soc.*, 2016, 138, 1922-1931.
35. D. E. DeRosha, B. Q. Mercado, G. Lukat-Rodgers, K. R. Rodgers and P. L. Holland, *Angew. Chem. Int. Ed.*, 2017, 56, 3211-3215.
36. B. Mondal, J. Song, F. Neese and S. Ye, *Curr. Opin. Chem. Biol.*, 2015, 25, 103-109.
37. J. Agarwal, B. C. Sanders, E. Fujita, H. F. Schaefer Iii, T. C. Harrop and J. T. Muckerman, *Chem. Commun.*, 2012, 48, 6797-6799.

38. A. Ariafard, N. J. Brookes, R. Stranger, P. D. W. Boyd and B. F. Yates, *Inorg. Chem.*, 2010, 49, 7773-7782.
39. C. Liu, L. Munjanja, T. R. Cundari and A. K. Wilson, *J. Phys. Chem. A*, 2010, 114, 6207-6216.
40. C. Liu, T. R. Cundari and A. K. Wilson, *Inorg. Chem.*, 2011, 50, 8782-8789.
41. V. Canale, R. Robinson, A. Zavras, G. N. Khairallah, N. d'Alessandro, B. F. Yates and R. A. J. O'Hair, *J. Phys. Chem. Lett.*, 2016, 7, 1934-1938.
42. J. Agarwal, E. Fujita, H. F. Schaefer and J. T. Muckerman, *J. Am. Chem. Soc.*, 2012, 134, 5180-5186.